Neglecting model parametric uncertainty can drastically underestimate flood risks

Sanjib Sharma[1,1,1], Benjamin Seiyon Lee[2,2,2], Iman Hosseini-Shakib[1,1,1], Murali Haran[1,1,1], and Klaus Keller[3,3,3]

[1]Pennsylvania State University
[2]George Mason University
[3]Thayer School of Engineering at Dartmouth College

December 7, 2022

Abstract

Floods drive dynamic and deeply uncertain risks for people and infrastructures. Uncertainty characterization is a crucial step in improving the predictive understanding of multi-sector dynamics and the design of risk-management strategies. Current approaches to estimate flood hazards often sample only a relatively small subset of the known unknowns, for example the uncertainties surrounding the model parameters. This approach neglects the impacts of key uncertainties on hazards and system dynamics. Here we mainstream a recently developed method for Bayesian inference to calibrate a computationally expensive distributed hydrologic model. We compare three different calibration approaches: (1) stepwise line search, (2) precalibration or screening, and (3) the new Fast Model Calibrations (FaMoS) approach. FaMoS deploys a particle-based approach that takes advantage of the massive parallelization afforded by modern high-performance computing systems. We quantify how neglecting parametric uncertainty and data discrepancy can drastically underestimate extreme flood events and risks. Precalibration improves prediction skill score over a stepwise line search. The Bayesian calibration improves the uncertainty characterization of model parameters and flood risk projections.

Posted on 7 Dec 2022 — CC-BY 4.0 — https://doi.org/10.1002/essoar.10510275.3 — This a preprint and has not been peer reviewed. Data may be preliminary.

Neglecting model parametric uncertainty can drastically underestimate flood risks

Sanjib Sharma[1], Benjamin Seiyon Lee[2], Iman Hosseini-Shakib[1], Murali Haran[3], and Klaus Keller[4]

[1]Earth and Environmental Systems Institute, Pennsylvania State University, University Park, PA, USA
[2]Department of Statistics, George Mason University, Fairfax, VA, USA
[3]Department of Statistics, Pennsylvania State University, University Park, PA, USA
[4]Thayer School of Engineering at Dartmouth College, Hanover, NH, USA

Corresponding author: Sanjib Sharma (svs6308@psu.edu)

Key points:

- We implement a sequential Monte Carlo particle-based Fast Model Calibrations (FaMoS) approach to improve the characterization of distributed hydrologic model parameters.
- FaMos demonstrates a relatively higher prediction skill than stepwise line search and precalibration.
- Accounting for model parametric uncertainty and observation errors can improve the uncertainty characterization of flood-damage projections.

Abstract

Floods drive dynamic and deeply uncertain risks for people and infrastructures. Uncertainty characterization is a crucial step in improving the predictive understanding of multi-sector dynamics and the design of risk-management strategies. Current approaches to estimate flood hazards often sample only a relatively small subset of the known unknowns, for example the uncertainties surrounding the model parameters. This approach neglects the impacts of key uncertainties on hazards and system dynamics. Here we mainstream a recently developed method for Bayesian inference to calibrate a computationally expensive distributed hydrologic model. We compare three different calibration approaches: (1) stepwise line search, (2) precalibration or screening, and (3) the Fast Model Calibrations (FaMoS) approach. FaMoS deploys a particle-based approach that takes advantage of the massive parallelization afforded by modern high-performance computing systems. We quantify how neglecting parametric uncertainty and data discrepancy can drastically underestimate extreme flood events and risks. Precalibration improves prediction skill score over a stepwise line search. The Bayesian calibration improves the uncertainty characterization of model parameters and flood risk projections.

1. Motivation and Introduction

Floods pose major risks to people and property (Alfieri et al., 2017; Wing et al., 2018; Winsemius et al., 2015). These risks are dynamic and deeply uncertain (Merz et al., 2010; Read & Vogel, 2015; Ruckert et al., 2019; Zarekarizi et al., 2020). It is important to characterize the uncertainties surrounding flood hazards in order to understand the impacts on multi-sector dynamics and to inform the design of risk-management strategies (Boulange et al., 2021; Chester et al., 2020; Liu & Merwade, 2018; Salas et al., 2018b; Wasko et al., 2021; Wong & Keller, 2017).

Hydrologic models are commonly used to understand hydrological processes, predict the response of hydrological systems to changing stresses, and provide boundary conditions to estimate flood hazards and risks (Bates et al., 2021; Brunner et al., 2020; Judi et al., 2018; Koren et al., 2004; Rajib et al., 2020; Thorstensen et al., 2016). However, hydrologic projections are subject to uncertainties such as from model structures, parameters and forcings (Gupta et al., 2012; Kavetski et al., 2006; Beven, 2014; Fisher & Koven, 2020; Hu et al., 2019; Mendoza et al., 2015). Parametric uncertainty can arise, for example, from the epistemic uncertainties about model parameters (Vrugt et al., 2003), the associated prior distributions (Tang et al., 2016), spatial-resolutions and objective functions (Melsen et al., 2019), and different choices of calibration approaches (Kavetski et al., 2018). Hydrologic models need to resolve the complex response of multiple processes (e.g., land surface characteristics, soil properties and climate variability) with strong nonlinear interactions and often few observations. Characterizing parametric uncertainty can be critical to improve prediction credibility and inform decision-making, for example, in the context of water-resources planning and flood-risk management (Herman et al., 2013; Ruckert et al., 2019; Wong & Keller, 2017; Zarekarizi et al., 2020).

Previous studies provide valuable new insights on flood hazard and risk estimates using model simulations (Bates et al., 2021; Judi et al., 2018; Rajib et al., 2020; Sanders et al., 2020; Sharma et al., 2021; Wing et al., 2018). For example, Judi et al. (2018) demonstrates an integrated multimodel multiscale simulation approach to evaluate social, economic, and infrastructure resilience to future flooding. Rajib et al. (2020) develops a coupled land surface hydrologic and river hydraulic modeling framework to provide regional flood hazard and risk estimates. Bates et al. (2021) presents estimates of current and future flood risk for all properties in the conterminous United States using a combined modeling approach considering river, coastal, or rainfall flooding. These studies typically obtain an optimal parameter set that produces the best possible agreement

between simulated and observed streamflow hydrographs at target locations. These previous studies break important new ground, but are mostly silent on the impacts of parametric uncertainties on hazards and dynamics. Neglecting parametric uncertainties can underestimate the tails of flood hazard probability distribution (Bates et al., 2021; Mendoza et al., 2015; Rojas et al., 2020; Salas et al., 2018a), and can result in poor decisions and outcomes (Ruckert et al., 2019; Wong & Keller, 2017; Zarekarizi et al., 2020).

Several studies on hydrologic model calibration have focused on manually adjusting a subset of model parameters (Bitew & Gebremichael, 2011; Siddique & Mejia, 2017). These manual calibrations typically rely on visual inspection of streamflow hydrograph and a trial and error-based procedure; hence, this method can be rather labor-intensive and time-consuming (Lahmers et al., 2021; Siddique & Mejia, 2017). A conceptual intuitive and relatively simple to implement approach for uncertainty characterization is the Generalized Likelihood Uncertainty Estimation (GLUE) method (Beven and Binley, 1992). The GLUE method has many advantages and can provide very useful insights, but several studies point to potential improvements with regard to subjective decisions on the likelihood function and implementing a statistically consistent error model (Blasone et al., 2008; Stedinger et al., 2008). A more complex approach adopted in this area is automatic parameter optimization (Kamali et al., 2013; Van Liew et al., 2005). Automatic calibration relies on systematic search approaches to find the best parameter values based on predefined single- and/or multi-objective functions (Kamali et al., 2013). Some studies use surrogate methods such as Gaussian process-based emulators to help identify best-fit parameters (Gou et al., 2020; Pianosi et al., 2016; Razavi & Tolson, 2013). Gou et al. (2020) presents an automatic calibration framework that combines sensitivity analysis and surrogate-based optimization for calibrating catchment-specific hydrologic model parameters. Surrogate-based methods are typically limited to cases with relatively fewer model parameters because training a surrogate model can be computationally prohibitive with high-dimensional inputs due to the large number of training data required (Hwang & Martins, 2018; Lee et al., 2020; Liu & Guillas, 2017) or repeated evaluations of the gradient of the model output with respect to the input parameters (Constantine et al., 2014; Lataniotis et al., 2020).

Bayesian calibration of hydrologic models have become increasingly popular (Hsu et al., 2009; Jeremiah et al., 2011; Kavetski et al., 2018; Raje & Krishnan, 2012; Razavi & Tolson, 2013; Shafii et al., 2015; Su et al., 2018; Zhu et al., 2018). For example, Vrugt et al., (2008) employ an

adaptive Metropolis Markov chain Monte Carlo (MCMC) sampling scheme-Differential Evolution Adaptive Metropolis (DREAM) algorithm to explore the entire parameter space of a hydrologic model. Different variants of DREAM algorithm (Vrugt et al., 2008; Vrugt et al., 2009; Laloy and Vrugt, 2012) demonstrate the value of Bayesian approaches on model calibration. Jeremiah et al. (2011) demonstrate an improved efficiency of Sequential Monte Carlo approach over the Adaptive Metropolis MCMC samplers in exploring the parameter space where the optimal solutions lie in the tails of the prescribed prior distribution. Su et al. (2018) uses a Bayesian hierarchical model to calibrate the Priestly–Taylor Jet Propulsion Laboratory model using observed evapotranspiration measurements. Given the relatively short model run times, the hierarchical model can be fit using the Differential Evolution Markov Chain (Braak, 2006; Storn & Price, 1997), a population MCMC algorithm. Zhu et al. (2018) calibrates eight parameters of a conceptual water balance model using a Particle Evolution Metropolis Sequential Monte Carlo (PEM-SMC). The PEM-SMC algorithm evaluates the water balance model 2, 000 times sequentially, which may be computationally prohibitive for distributed hydrologic models with longer run times. These studies break important new ground, but focus on calibrating (1) average response of process over the watershed using a lumped hydrological model; (2) limited number of model parameters; (3) low-to-moderate flow threshold; and (4) relatively small basins. However, the computational requirement can be drastically larger for fully distributed hydrological modeling over the large basin and with a large number of sensitive parameters.

Here we expand on previous studies and demonstrate an implementation of a Bayesian model calibration framework by: (1) considering a computationally expensive distributed hydrologic model; (2) taking advantage of the massive parallelization afforded by modern high-performance computing systems; (3) focusing on a large number of extreme streamflow events; (4) characterizing model parametric uncertainty, and (5) assessing the impacts of uncertainty characterization on projected flood-hazards and -risks.

2. Bayesian Model Calibration

Various algorithms exist for characterizing hydrologic model parametric uncertainty, including the multicriteria approach (Gupta et al., 1998), Generalized likelihood Uncertainty Estimation (GLUE) (Beven and Binley, 1992), Shuffled Complex Evolution Metropolis algorithm (SCEM-UA) (Duan et al., 1992; Sorooshian et al., 1993), Shuffled Complex Evolution Metropolis

(SCEM-UA) algorithm (Vrugt et al., 2003), and Differential Evolution Adaptive Metropolis (DREAM) (Vrugt 2008; Laloy and Vrugt 2012; Vrugt et al., 2009), among others.

Bayesian computer model calibration (Bayarri et al., 2007a; Higdon et al., 2004; Kennedy & O'Hagan, 2001; Sacks et al., 1989) typically addresses several (potentially overlapping) objectives: (1) estimate the input parameters (in other words: what is the best parameter estimates); (2) quantify the parametric uncertainty (in other words: what is the joint probability density function of the parameters); and (3) infer the parameters of the observational error model and discrepancy terms. These parameter estimates are impacted by factors such as model-observation discrepancy (Bayarri et al., 2007b; Brynjarsdóttir & O'Hagan, 2014; Kennedy & O'Hagan, 2001) and measurement errors. The Bayesian model calibration framework (see the discussion in Kennedy and O'Hagan, 2001) facilitates both parameter estimation and uncertainty quantification while also accounting for external sources of uncertainty (e.g., discrepancy and measurement errors). For each model parameter, we specify prior distributions based on expert knowledge and then update the priors by comparing the model runs to the observed data. The update proceeds by placing more weight on the parameter sets whose corresponding model runs align better with the observations. The resulting posterior (updated) distribution naturally provides both point and interval estimates of the model parameters in light of the newly acquired data. Let $\boldsymbol{\theta}$ be the vector of the model parameters, σ^2 the variance of the (assumed) independent and identically distributed observational error, and $\boldsymbol{\delta}$ the discrepancy term. The posterior distribution $\tilde{\pi}(\boldsymbol{\theta}, \sigma^2, \boldsymbol{\delta}|\, \boldsymbol{Z})$ is defined as:

$$\tilde{\pi}(\boldsymbol{\theta}, \sigma^2, \boldsymbol{\delta}|\, \boldsymbol{Z}) \propto L(\boldsymbol{\theta}, \sigma^2, \boldsymbol{\delta}|\boldsymbol{Z}) \times \pi(\boldsymbol{\theta}) \times \pi(\sigma^2) \times \pi(\boldsymbol{\delta}),$$

where $\tilde{\pi}(\boldsymbol{\theta}, \sigma^2, \boldsymbol{\delta}|\, \boldsymbol{Z})$ and $\pi(\cdot)$ denotes the probability density function of the posterior and prior distributions, respectively. $L(\boldsymbol{\theta}, \sigma^2, \boldsymbol{\delta}|\boldsymbol{Z})$ is the likelihood function based upon the hydrological model output, discrepancy term, and the observational error model (see Appendix).

For complex deterministic models, the posterior distribution may not be available in closed form (Higdon, 2003; Oakley, 2009). In this case, a common approach is to approximate the posterior via sampling approaches such as Markov chain Monte Carlo (MCMC) or Sequential Monte Carlo. The choice of sampling approaches in influenced by several factors including: (1) the computational time requirements for a single model evaluation; (2) the number of model parameters to be calibrated, (3) the degree to which the algorithm can be parallelized, (4) the available computation environment, and (5) the available time for the computations. Markov chain

Monte Carlo methods with the true model can be an excellent choice for models with short single model run times (Asher et al., 2015; Gramacy, 2020; Lee et al., 2020). Surrogate modeling (i.e. emulation-calibration) approaches replace the hydrologic model with a faster surrogate model within the calibration framework; however, constructing a high-fidelity surrogate model may be computationally prohibitive for high-dimensional input spaces (X. Liu and Guillas 2017; Gramacy 2020). Sequential Monte Carlo (SMC) (Lee et al. 2020; Kalyanaraman et al. 2016; Papaioannou, Papadimitriou, and Straub 2016; Kantas, Beskos, and Jasra 2014; Morzfeld et al. 2018) methods can be a practical alternative for calibrating hydrological models with a larger number of input parameters.

2.1. The Fast Model Calibrations (FaMoS) approach

We use a sequential Monte Carlo particle-based approach that relies on massive parallelization afforded by a high-performance computing system to efficiently calibrate a distributed hydrologic model in a relatively large watershed with a number of extreme events.

Fast **M**odel Calibration**s** (FaMoS) approach (Lee et al., 2020) provides an approximation of the posterior distribution by (i) generating an adaptive posterior incorporation schedule to preserve particle diversity; (ii) requiring very few Metropolis-Hastings updates in the mutation stages; and (iii) lending itself to parallel operations distributed across thousands of processors. We provide technical details about FaMoS in the Appendix.

FaMoS approximates the posterior distribution of the model parameters using a series of sampling, reweighting, and re-sampling steps. The basic premise of sampling-importance resampling (Gordon et al., 1993) is to draw independent samples from the model parameters' prior distribution and retain the parameter sets whose corresponding outputs closely resemble the actual observations. Each parameter set is then assigned weights, which are proportional to the likelihood function L($\boldsymbol{\theta}$|Z). The parameter sets whose model outputs fit the observed data well are given larger weights and those that do not are assigned smaller weights. The (importance) weights $w(\boldsymbol{\theta})$ are defined as:

$$w(\boldsymbol{\theta}) = \frac{f(\boldsymbol{\theta})}{q(\boldsymbol{\theta})} = \frac{\tilde{\pi}(\boldsymbol{\theta}|Z)}{\pi(\boldsymbol{\theta})}, \quad (1)$$

where $f(\boldsymbol{\theta})$ is the target function and $q(\boldsymbol{\theta})$is the importance function. In this context, we specify the target function as the posterior distribution of the model parameters $\tilde{\pi}(\boldsymbol{\theta}|\boldsymbol{Z})$ and importance

function as the prior distribution of the parameters $\pi(\boldsymbol{\theta})$. We approximate $\tilde{\pi}(\boldsymbol{\theta}|\boldsymbol{Z})$ using the weighted empirical distribution $\hat{\pi}(\boldsymbol{\theta}|\boldsymbol{Z})$ defined as:

$$\tilde{\pi}(\boldsymbol{\theta}|Z) \approx \hat{\pi}(\boldsymbol{\theta}|\boldsymbol{Z}) = \sum_{i=1}^{N} w\,(\boldsymbol{\theta}^{(i)})\delta(\boldsymbol{\theta}^{(i)})\,, \qquad (2)$$

where $w(\boldsymbol{\theta}^{(i)})$is the importance weight and $\delta\left(\boldsymbol{\theta}^{(i)}\right)$is a Dirac measure at $\boldsymbol{\theta}^{(i)}$ for the i-th sample.

In the fast particle-based approach (Lee et al. 2020), we draw an initial ensemble of model parameters (particles) from the prior distribution (i.e., importance function) and approximate the posterior distribution (target function) using the initial ensemble. When there is very little overlap in the high-probability regions of the prior and posterior distribution, the initial ensemble may not adequately approximate the posterior distribution due to: (1) weight degeneracy, where the vast majority of particles have near-zero weights; and (2) sample impoverishment, where we "resample" the existing particles based on the weights, and we are left with multiple copies of a few unique particles. When there is very little overlap in the high-probability regions of the prior and posterior distribution, the initial ensemble may not adequately approximate the posterior distribution due to: (1) weight degeneracy, where the vast majority of particles have near-zero weights; and (2) sample impoverishment. Sample impoverishment occurs when we are left with multiple copies of a few unique particles after a "resampling" stage. In FaMoS, the resulting particles are "resampled" through multinomial sampling based on the importance weights w($\boldsymbol{\theta}$i) then "mutated" or "jittered" using Metropolis-Hastings updates. Please see the Appendix for additional details.

FaMoS (Lee et al, 2020) mitigates these issues by gradually building up to the posterior distribution, a technique from iterated batch importance sampling (Chopin, 2002) and Sequential Monte Carlo. Here, we consider a series of intermediate posterior distributions where those earlier in the series closely resemble the prior distribution and those at the latter part better resemble the full posterior distribution. In the first cycle, we use particles from the prior distribution to approximate an earlier intermediate posterior distribution. In the subsequent cycles, we use samples from an intermediate posterior distribution to approximate a later intermediate posterior distribution. We end the algorithm when the target distribution is the final posterior distribution. For cycles t=1,...,T, the t-th intermediate posterior distribution is:

$$\tilde{\pi}_t(\boldsymbol{\theta}|\,\boldsymbol{Z}) \;\propto\; L(|\boldsymbol{Z})^{\gamma_t} \;\times\; \pi(\boldsymbol{\theta}), \qquad (3)$$

where $\gamma_t$denotes the incorporation factor such that $0 = \gamma_0 \leq \gamma_1 \leq \ldots \leq \gamma_{T-1} \leq \gamma_T = 1$. Note that the 0-th intermediate posterior distribution ($\tilde{\pi}_0(\boldsymbol{\theta}|\,\boldsymbol{Z})$) is simply the prior distribution $\pi(\boldsymbol{\theta})$ with

incorporation factor $\gamma_0 = 0$. Likewise, the T-th intermediate posterior distribution $\tilde{\pi}_T(\boldsymbol{\theta}|\boldsymbol{Z})$ is the full posterior distribution since $\gamma_T = 1$. At each time *t*, the target distribution is the *t*-th intermediate posterior distribution $\tilde{\pi}_t(\boldsymbol{\theta}|\boldsymbol{Z})$, and the prior is the intermediate posterior from the previous iteration $\tilde{\pi}_{t-1}(\boldsymbol{\theta}|\boldsymbol{Z})$.

At the end of each cycle, there still may be many replicates of a few unique particles, or sample impoverishment. To increase the number of unique particles, we "jitter" or "mutate" the particles through a carefully constructed kernel function (Gilks & Berzuini, 2001; Li et al., 2014; Liu & West, 2001). To increase the number of unique particles at the end of each cycle (*t*), we "jitter" or "mutate" the particles through a carefully constructed kernel function (Gilks & Berzuini, 2001; Li et al., 2014; Liu & West, 2001). Upon completion of the fast particle-based calibration algorithm, we are left with an ensemble of updated parameter sets (particles) which sensibly approximate the posterior distribution. Lee et. al. (2020) also provides guidelines for choosing the number of cycles, how to mutate the particles, and how to construct these intermediate posterior distributions. We approximate the posterior distribution using "mutated" samples from the final (T-th) intermediate posterior distribution:

$$\tilde{\pi}(\boldsymbol{\theta}|\boldsymbol{Z}) = \tilde{\pi}_T(\boldsymbol{\theta}|\boldsymbol{Z}) \approx \sum_{i=1}^{N} w_T(\widehat{\boldsymbol{\theta}}^{(i)})\delta(\widehat{\boldsymbol{\theta}}^{(i)}) \quad (4)$$

where $\widehat{\boldsymbol{\theta}}^{(i)}$ is the i-th mutated particle, $w_T(\widehat{\boldsymbol{\theta}}^{(i)})$ are the corresponding weights from the T-th cycle, and $\delta(\widehat{\boldsymbol{\theta}}^{(i)})$is a Dirac measure at $\widehat{\boldsymbol{\theta}}^{(i)}$.

3. Experimental Design

We demonstrate the approach for a case study in the Susquehanna River basin, Pennsylvania, United States. Pennsylvania provides a relevant study area as it ranked second, tenth, and fourteenth in the United States in terms of the frequency of flash flood-related fatalities, injuries, and casualties in 1959-2005 (Ashley & Ashley, 2008). This region has experienced several devastating flooding events over the recent decades, including floods associated with the remnants of Hurricane Ivan (September 2004), late winter–early spring extratropical systems (April 2005), warm-season convective systems (June 2006), and tropical storm Lee (September 2011) (Gitro et al., 2014; Grumm, 2011). In Pennsylvania, the Federal Emergency Management Agency (FEMA) paid $953 million in property damages to National Flood Insurance Program participants between 1975 and 2019 (FEMA, 2019).

We use the National Oceanic and Atmospheric Administration's (NOAA) Hydrology Laboratory-Research Distributed Hydrologic Model (HL-RDHM) (Koren et al., 2004). Distributed hydrologic modeling accounts for the spatial variability of model inputs, parameters and states to analyze rainfall-runoff processes at desired locations within a river basin. Distributed modelling involves processing and storing large amounts of data required to solve numerous and complex physics-based equations at each grid cell. We run HL-RDHM in a fully distributed mode at a spatial resolution of 2 km. The 2×2 km^2 resolution mainly allows for a more realistic representation of the stream network. Within HL-RDHM, we use the Sacramento Soil Moisture Accounting model with Heat Transfer (SAC-HT) (Koren et al., 2004) to represent hillslope rainfall-runoff processes, and the SNOW-17 module (Anderson et al., 2006) to represent snow accumulation and melt. SAC-HT is a physics-based, conceptual model where the basin system is divided into regularly spaced, square grid cells to account for spatial heterogeneity and variability. Each grid cell, in turn, is composed of storage components that store and transmit water. The cells are ultimately connected to each other through the stream network system, that is, each cell acts as a hillslope capable of generating surface and subsurface runoff that discharges directly into the streams. The hillslope runoff, generated at each grid cell by the SAC-HT and SNOW-17, is routed to the stream network using a nonlinear kinematic wave algorithm (Koren et al., 2004). Further information about the HL-RDHM model can be found for example in Koren et al. (2004), Reed et al. (2004), and Anderson et al. (2006). The HL-RDHM distributed hydrological model takes approximately 15 minutes per run on a single 2.3-GHz Intel Xeon E5-2697V4 (Broadwell) processor on the Cheyenne cluster (Computational and Information Systems Laboratory, 2017).

We use three main datasets: multisensor precipitation estimates, gridded near-surface air temperature, and streamflow. We use NOAA's multisensor precipitation estimates and gridded near-surface air temperature products to run the hydrological model for parameter calibration purposes and to initialize the model. Multisensor precipitation estimates represent a continuous time series of hourly, gridded precipitation observations at 4×4 km^2 cells, which are produced by combining multiple radar estimates and *in situ* rain-gauge measurements (Prat & Nelson, 2015; Rafieeinasab et al., 2015). The gridded near-surface air temperature data are derived by combining multiple temperature observation networks, including the meteorological terminal aviation routine weather report (METAR), USGS stations, and National Weather Service Cooperative Observer Program (Siddique & Mejia, 2017). We use streamflow observations from the United States

285 Geological Survey gage 01554000 located at Susquehanna River at Sunbury, Pennsylvania. The
286 selected gage station represents the drainage area of 47, 396 km^2.
287 We calibrate the model for the period of 2004-2008 and use 2009-2012 observations to
288 evaluate the calibration performance. We use the year 2003 to spin up the model. As part of the
289 calibration process, we select 12 out of the 17 model parameters associated with each model grid
290 cell (Table S1). To improve calibration efficiency, basin-scale parameter multipliers, rather than
291 the parameters in each grid, were calibrated and applied to the a-priori parameter grids (NWS,
292 2011). We only consider the model parameters that have a strong influence on the model output
293 (see Figure S1). Exploring a higher-dimensional parameter space demands additional processors
294 (particles) (Bain & Crisan, 2008; Jeremiah et al., 2011; Kantas et al., 2014) to sensibly calibrate
295 the hydrological model. Selecting only the strongly influential model parameters can help reduce
296 the computational costs considerably. This is, of course, an approximation and points to future
297 research needs. The sensitive parameters are associated with different hydrodynamic processes
298 related to baseflow, percolation, evaporation, snowfall, storm runoff, and channel routing (Table
299 S1). These parameters are also suggested by several other studies (Gomez et al., 2019; Sharma et
300 al., 2021; Siddique & Mejia, 2017; Zarzar et al., 2018) as the most sensitive parameters in the
301 Susquehanna river basin.
302 We compare Bayesian calibration with relatively simple and low-cost model calibration
303 approaches: i) stepwise line search (Kuzmin et al., 2008) and ii) precalibration (Edwards et al.,
304 2011). Stepwise line search typically adjusts a subset of model parameters to minimize an objective
305 function (e.g., root mean square error) and returns a single estimate of the model parameters (for
306 details of the implementation please see Text S2) (Bowman et al., 2017; Carlberg et al., 2020;
307 Fares et al., 2014; Mejia & Reed, 2011; Siddique & Mejia, 2017). Precalibration applies a
308 screening criterion to a large ensemble of hydrologic model runs and rules out any implausible
309 model runs that deviate substantially from the observations (refer Text S3 for the details) (Craig
310 et al., 1997; Edwards et al., 2011; Holden et al., 2010; Williamson et al., 2017; Edwards et al.,
311 2019). The Bayesian analogue to the stepwise line search could be the maximum *a posteriori*
312 estimate. However, both estimators use a different objective function and possibly result in
313 different estimates. Precalibration is a sampling-based method without any specification of a
314 likelihood function. These simple approaches of carrying out limited calibration are used by many
315 academic studies (Rafieeinasab et al., 2015; Siddique and Mejia, 2017; Fares et al., 2014; Kim et

316 a., 2021; Mayr et al., 2013; Tarawneh et al., 2016; Li et al., 2019) as well as commonly practiced
317 in real-word applications (Salas et al., 2018). They are used in part because they are simple and
318 fast (Knutti et al., 2002; Reed et al., 2022).
319 We evaluate the calibrated model performance using several decision-relevant metrics. We
320 use traditional deterministic metrics such as the Kling-Gupta Efficiency (KGE) (Mizukami et al.,
321 2019), which provides a direct assessment of streamflow time series (e.g., shape, timing, water
322 balance and variability) using the ensemble mean estimate. We also evaluate the probabilistic
323 prediction skill using the Brier Skill Score (BSS) (Murphy, 1973) and the Continuous Ranked
324 Probability Skill Score (CRPSS) (Murphy, 1970). The Brier score is essentially the mean squared
325 error of the probability predictions, considering that the observation is one if the event occurs, and
326 that the observation is zero if the event does not occur. The Continuous Ranked Probability Score
327 measures the integral square difference between the cumulative distribution functions of the
328 observation and predictions, averaged over all pairs of predictions and observations. The selection
329 of these decision-relevant metrics is motivated by the balance between model output goodness-of-
330 fit, calibration approaches, and data availability. The description of evaluation metrics is provided
331 in Text S4 in the supporting information. Model calibration and evaluation is focused on high
332 flows by choosing the river flow that exceeds NOAA's Action Stage (McEnery et al., 2005).
333 Action Stage refers to the stage which, when reached by a rising river, represents the level where
334 the National Weather Service or a partner/user needs to take some mitigation action in preparation
335 for possible significant hydrologic activity.
336 We assess the impact of model calibration on flood damage estimates. Flood damage
337 represents interactions among hazard, exposure and vulnerability (Tellman et al., 2021; Wing et
338 al., 2018). Hazard in this case refers to the magnitude of the flood event. Exposure characterizes
339 property value in the floodplain. Vulnerability characterizes how sensitive the impacts are for a
340 given hazard and exposure. We consider 2,000 hypothetical houses to quantify the damage from
341 flood hazards (Figure S4; TextS6). We assess damage for a certain depth of water in a house by
342 using a relatively simple Bathtub-based flood inundation model (Didier et al., 2019; Fereshtehpour
343 & Karamouz, 2018; Neumann & Ahrendt, 2013; Yunus et al., 2016) and a vulnerability model
344 (Scawthorn et al., 2006). The Bathtub model relies on a digital elevation model to provide flood
345 depth in a house for a particular corresponding water level in the river (refer TextS5 and TextS6

for the details). We use a common vulnerability model (depth-damage function) provided by the Federal Emergency Management Agency (FEMA) (Scawthorn et al., 2006).

4. Results and Discussion

We first generate streamflow simulations using the "best" parameter estimates obtained via the stepwise line search (Figure 2). In the considered example, stepwise line search substantially underestimates the high streamflow (Figure 2). Stepwise line is designed to sample high-probability outcomes and excludes comprehensive sampling of the parametric distribution (Kuzmin et al., 2008; Sharma et al., 2019).

We account for parametric uncertainty using precalibration and FaMoS (Figure S1). Characterizing parametric uncertainty requires knowledge of model behavior throughout the (often high-dimensional) parameter space. Precalibration provides a relatively simple method to explore the high-dimensional parameter space. Precalibration is a low-cost way of ruling out implausible model runs. We begin with an initial ensemble of 5,000 model runs with input parameters settings selected from a 12-dimensional Latin hypercube design (Helton & Davis, 2003). We select an ensemble of 165 runs that fall within the +/- 75% window surrounding each observation. Note that specifying bounds for precalibration is a subjective choice (Craig et al., 1997; Edwards et al., 2011; Holden et al., 2010; Tarawneh et al., 2016). This choice impacts the "surviving" parameter samples. For instance, imposing tight bounds on the observed streamflow could lead to high-resolution sampling of the plausible parameter space and wider bounds may include more implausible runs into the final ensemble. We choose the considered acceptable range to sample into the upper tails of projected flood hazards, which are often associated with high-cost events.

FaMoS adopts a more complex (but also more powerful) calibration approach compared to precalibration. We incorporate domain-area expertise (prior distribution) of the unknown parameters and also account for additional sources of uncertainty such as model-observation discrepancies and observational error (see the Appendix for the details). As a result, we obtain a distribution of viable parameter values (posterior distribution) along with interval estimates, as opposed to a single best fit estimate (Figure S1). Unlike precalibration, FaMoS does not fix an arbitrary screening criterion, but rather uses a flexible statistical model to assess model-fit. Moreover, FaMoS sequentially explores the entire parameter space and systematically attempts to

move to a "target" region that contains the most plausible sets of model parameters. In contrast, precalibration attempts to locate this "target" region using a single initial ensemble of model runs.

Accounting for parametric uncertainty improves model performance metrics for the calibration data and out-of-sample predictions (Figure 3). We compute the skill score (KGE, BSS, and CRPSS) with reference to raw (uncalibrated) model runs using default parameter estimates obtained from several previous studies (Anderson et al., 2006; Reed et al., 2007). In terms of the performance metrics, model predictions remain skillful for all the calibration approaches (Figure 3). Precalibration outperforms the stepwise line search (best estimate predictions). Stepwise line search and precalibration are not designed to find the global optimum, which can lead to worse skill score as compared to FaMoS. FaMoS demonstrate a higher skill score than both the stepwise line search and precalibration for both calibration and out-of-sample evaluations.

Accounting for parametric uncertainty improves flood hazard estimates (Figure 4). The resulting predictive distribution of flood events demonstrates the impacts of model calibration. The stepwise line search underestimates the flood peaks by as much as 35% (Figure 4b) during calibration and 40% during out-of-sample prediction (Figure 4e). Precalibration captures the specific flood events, but exhibits very high prediction uncertainty as evidenced by the wider prediction intervals. Overall, FaMoS improves flood peak estimates and provides narrower prediction intervals. Consider, as an example, the case of Tropical Storm Lee with streamflow observation of 11, 292 m^3/sec (Figure 4). Precalibration provides a flood peak prediction of 10, 539 m^3/sec and prediction intervals (5%-95% credible interval) range from 6, 359 m^3/sec to 14, 222 m^3/sec (width = 7, 863 m^3/sec). FaMoS has a corresponding flood peak prediction of 11, 467 m^3/sec with a credible interval ranging from 9, 925 m^3/sec to 13, 121 m^3/sec (width = 3, 196 m^3/sec). Sampling both the parametric uncertainty and observation errors can improve the uncertainty characterization of model parameters and flood peak predictions (refer Supporting Information Figures S4 and S5). However, the prediction intervals can be quite wide, leading to arguably unrealistic streamflow estimates. Incorporating a flexible observational-error model and a discrepancy term may improve the representation of the underlying error structure.

We assess each calibration approach's classification ability or how well each method discriminates between occurrences (water level crossing the action stage) versus non-occurrences (regular water level) of an event (Figure 5). Managing flood risks can require decision makers to choose between two options (e.g., to evacuate or not or to elevate a house or not) based on a

406 prediction of an event (e.g., water rising to a certain level) with one decision preferred if the event
407 doesn't occur, and the other if it does. A perfect prediction system for a binary outcome correctly
408 predicts the occurrence of an event (unity probability of detection) and never issues incorrect
409 predictions when it does not occur (zero probability of false detection). How well a prediction
410 system approaches this ideal case can be quantified by the relative operating characteristics (ROC)
411 curve (see Text S4) (Mason & Graham, 2002). Technically, the ROC curve assesses the quality of
412 probability predictions by relating the probability of detection (true alarm) to the corresponding
413 probability of false detection (false-alarm rate), as a decision threshold is varied across the full
414 range of a continuous prediction quantity (Figure 5). We fix the threshold corresponding to the
415 river flow that exceeds NOAA's Action Stage. Streamflow predictions obtained using FaMoS
416 parameter distribution exhibit better discriminatory ability (higher ROC score) than the stepwise
417 line search and precalibration. Stepwise line search shows a relatively poor ability to discriminate
418 between different events. This poor ability to discriminate between the events can lead to poor
419 decisions and outcomes.
420 Neglecting parametric uncertainty also underestimates potential flood damage (Figure 6). We
421 find that the stepwise line search tends to underestimate the flood damage. The underestimation
422 bias increases as flood magnitude increases. Accounting for parametric uncertainty improves the
423 damage estimates for the calibration data and out-of-sample predictions. The damage credible
424 interval obtained using FaMoS parameter distribution generally captures the observed damage for
425 different flood events. As expected, at the upper tails of the damage, the predictive uncertainty
426 tends to be higher for the out-of-sample prediction as compared to the calibration.
427
428 **5. Caveats**
429 We use a relatively simple model and small region with hypothetical exposure to demonstrate
430 our points. This parsimony helps with transparency, but it comes with several caveats. For
431 example, our analysis focuses on calibrating high flows by choosing the river flow that exceeds
432 NOAA's Action Stage. Temporal independence, conditioned on the model outputs, is a key
433 assumption within the calibration framework. We calibrate multiple disjoint (or unconnected)
434 instances of extreme streamflow events. We compute skill score to assess the performance of
435 different calibration approaches. However, implementing the Ljung-Box test and other diagnostic
436 tools for autocorrelation (Smith et al., 2015) would require calibrating a continuous streamflow

time series. Future work might consider calibrating a continuous time series of streamflow, including low flows and moderate flows. Due to a large number of low and moderate flow observations, dimension-reduction techniques like principal components (Chang et al., 2014; Higdon et al., 2008) or eigenfunctions (Mak et al., 2018) may be appropriate to summarize the large datasets. This study samples shallow uncertainty about hydrologic model parameters as a case-study. There are, of course, other deep uncertainties (Lempert, 2002) affecting flood hazards and risks that could be taken into account in future work (Mendoza et al., 2015, Bates et al., 2021, Reed et al., 2022). These include model structural uncertainty, different spatial resolutions, land surface characteristics, or projections of the socio-economic systems (Gupta et al., 2012; Kavetski et al., 2006; Zarekarizi et al., 2020). Characterizing the individual uncertainty sources and their propagation is crucial to improve the reliability of flood hazard and risk projections. Increasing the spatio-temporal resolutions may drastically raise the hydrologic model's complexity as well as the associated single model run times. To reduce the number of sequential hydrologic model evaluations, we can embed parallel Markov Chain Monte Carlo approaches such as Multiple-Try Metropolis (Liu et al., 2000) or "emcee" samplers (Goodman & Weare, 2010) or genetic algorithms (Park et al., 2009) into FaMoS calibration framework. We note that our damage estimates are based on a simple Bathtub-based flood inundation model. Future work could use process-informed models to characterize the impacts of hydrodynamic processes in damage estimates (Brunner, 1995; Coulthard et al., 2013; Judi et al., 2018). In addition, future work could sample the uncertainty surrounding the flood vulnerability of the building (Wing et al., 2020).

Although the objective of this study is not to compare different complex calibration approaches, FaMoS can add to emerging research into uncertainty quantification of a distributed hydrologic model. We demonstrate the ability of FaMoS to calibrate a large number of extreme flood events and consider a relatively larger river basin than in the several previous studies (Vrugt et al., 2008; Vrugt et al., 2009; Laloy and Vrugt, 2012). Computationally, the problem becomes very different to run and calibrate a spatially distributed model over a large river basin. Future study could compare FaMoS with other complex and state-of-the art Bayesian calibration approaches (e.g., Vrugt et al., 2008).

6. Conclusions

We use a Bayesian data-model fusion framework to calibrate a distributed hydrologic model and to demonstrate practical implications of neglecting key uncertainties on hazard- and risk-estimates. We compare the results of the Bayesian approach to two simpler methods: stepwise line search and precalibration. We show that these simpler methods can considerably underestimate flood hazards and risks. Precalibration improves flood hazards estimates over the best fit estimates, but provides a wider predictive interval (i.e., highly uncertain estimates) than the Bayesian approach. The predictive skill of the Bayesian approach dominates the stepwise line search and precalibration approaches. We show how neglecting model parametric uncertainty can substantially underestimate flood hazards and risk estimates and demonstrate how applying state-of-the-art statistical methods can help to refine flood-risk projections.

Acknowledgments

This study was co-supported by the US Department of Energy, Office of Science through the Program on Coupled Human and Earth Systems (PCHES) under DOE Cooperative Agreement No. DE-SC0016162 and DE-SC0022141 as well as the Penn State Center for Climate Risk Management. We thank Rob Nicholas, Skip Wishbone, Dave Judi, and the PSIRC team for inputs. All errors and opinions (unless cited) are those of the authors and not of the funding entities.

Disclaimer and License

The results, data, software tools, and other resources related to this work will be available under the GNU general public open-source license, as-is, without warranty of any kind, expressed or implied. In no event shall the authors or copyright holders be liable for any claim, damages, or other liability in connection with the use of these resources. This is academic research and not designed to be used to guide a specific decision.

Author contributions

All authors contributed to the study design. S.S. led the hydrologic analysis. B.L. and M.H. constructed the particle-based calibration model. I.H.S led the flood damage analysis. I.H.S. performed a code review. S.S., B.L, and K.K wrote the initial draft of the manuscript. All authors revised and edited the manuscript.

Data and Code Availability

The code used for this analysis and the data required to plot the results is available through a publicly accessible GitHub repository and under the GNU open-access license upon acceptance to a peer-reviewed journal. Reviewers can access these resources from https://github.com/benee55/FamosHydroModel. All data and code currently available at GitHub will be published via Zenodo upon article acceptance.

Competing interests

The authors are not aware of any competing financial or nonfinancial interests.

Materials & Correspondence

Correspondence and requests for materials should be addressed to the corresponding author. The code and data are available on GitHub (made public upon acceptance of the paper).

List of Figures

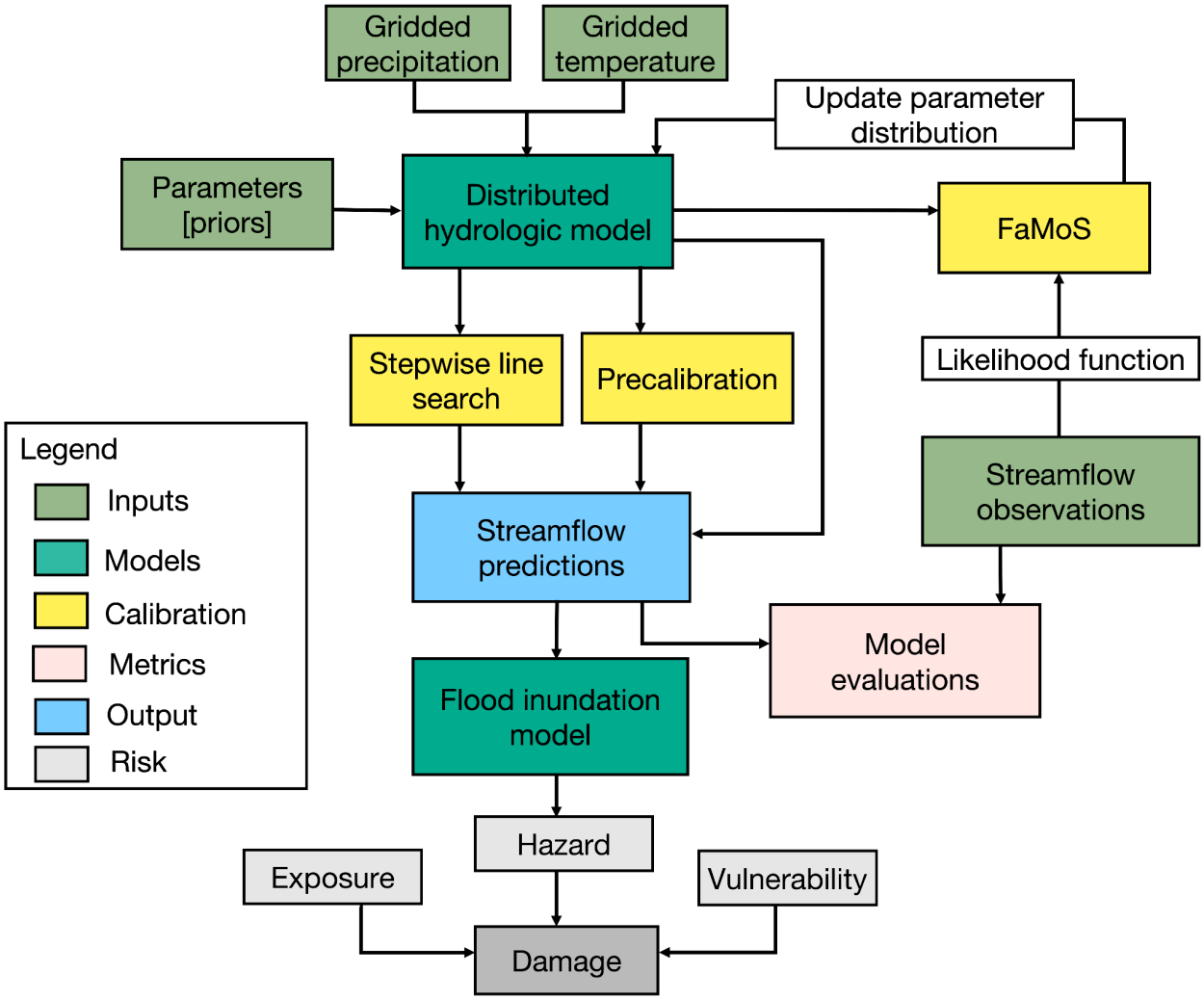

Figure 1: Diagrammatic representation of distributed hydrological model calibration framework. The framework also demonstrates flood hazards and risk components.

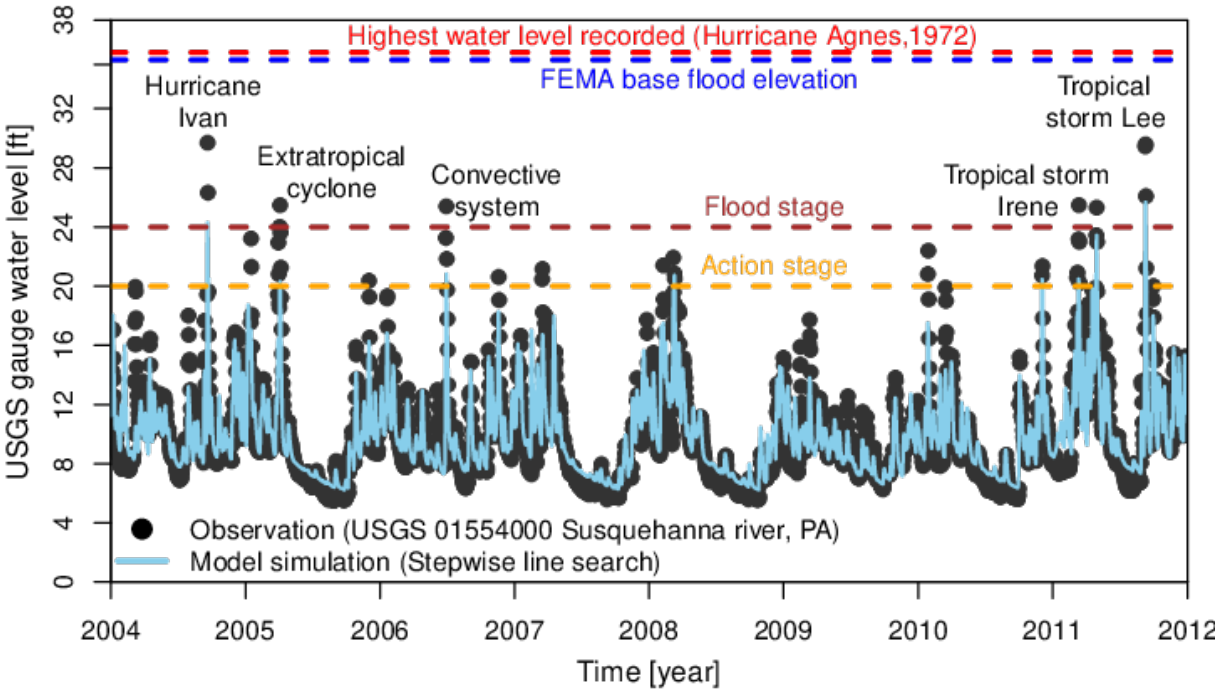

516

517 **Figure 2:** Historical time series of water level observation and model simulations obtained using
518 best parameter estimates (stepwise line search). We obtain the observation from the United States
519 Geological Survey (USGS) gauge records for ID 01554000 located upstream of Selinsgrove,
520 Pennsylvania, USA. The most destructive floods in the Susquehanna River basin that occurred in
521 recent years, each associated with different flood-generating mechanisms, includes Hurricane Ivan
522 (September 2004), late winter–early spring extratropical systems (April 2005), warm-season
523 convective systems (June 2006), and tropical storm Lee (September 2011).

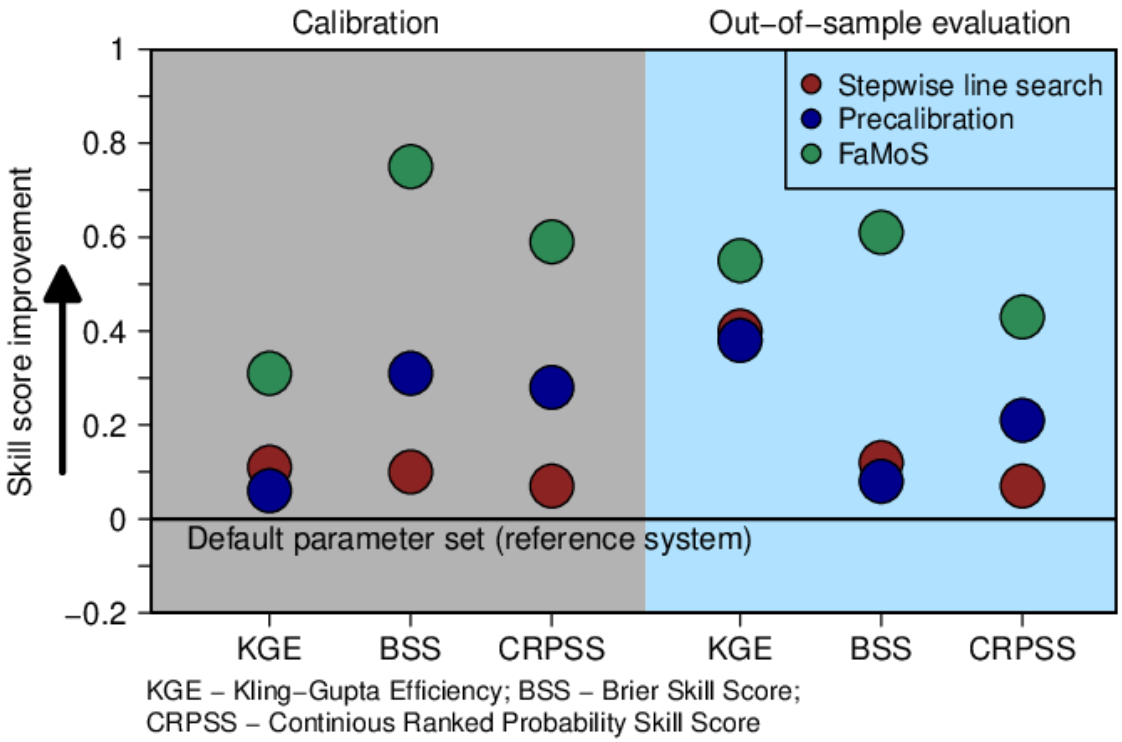

Figure 3: Performance metrics for hydrological model calibration and out-of-sample prediction. We compute Kling-Gupta Efficiency (KGE), and Brier skill score (BSS), and mean Continuous ranked probability skill score (CRPSS). All the metrics are computed with reference to the default parameter set available from several previous studies (Anderson et al. 2006, Reed et al. 2004). Any positive values of the skill score, from 0 to 1, indicate that the calibration approach performs better than the reference system. Thus, a skill score of zero indicates no skill, and a skill of one indicates perfect skill. We plot the average value to compute KGE. CRPSS measures the integrated squared difference between the cumulative distribution function (cdf) of a model prediction, and the corresponding cdf of the observations. The CRPSS is averaged across n pairs of model predictions and observations, which leads to the mean CRPSS. BSS measures the averaged squared error of a probability prediction.

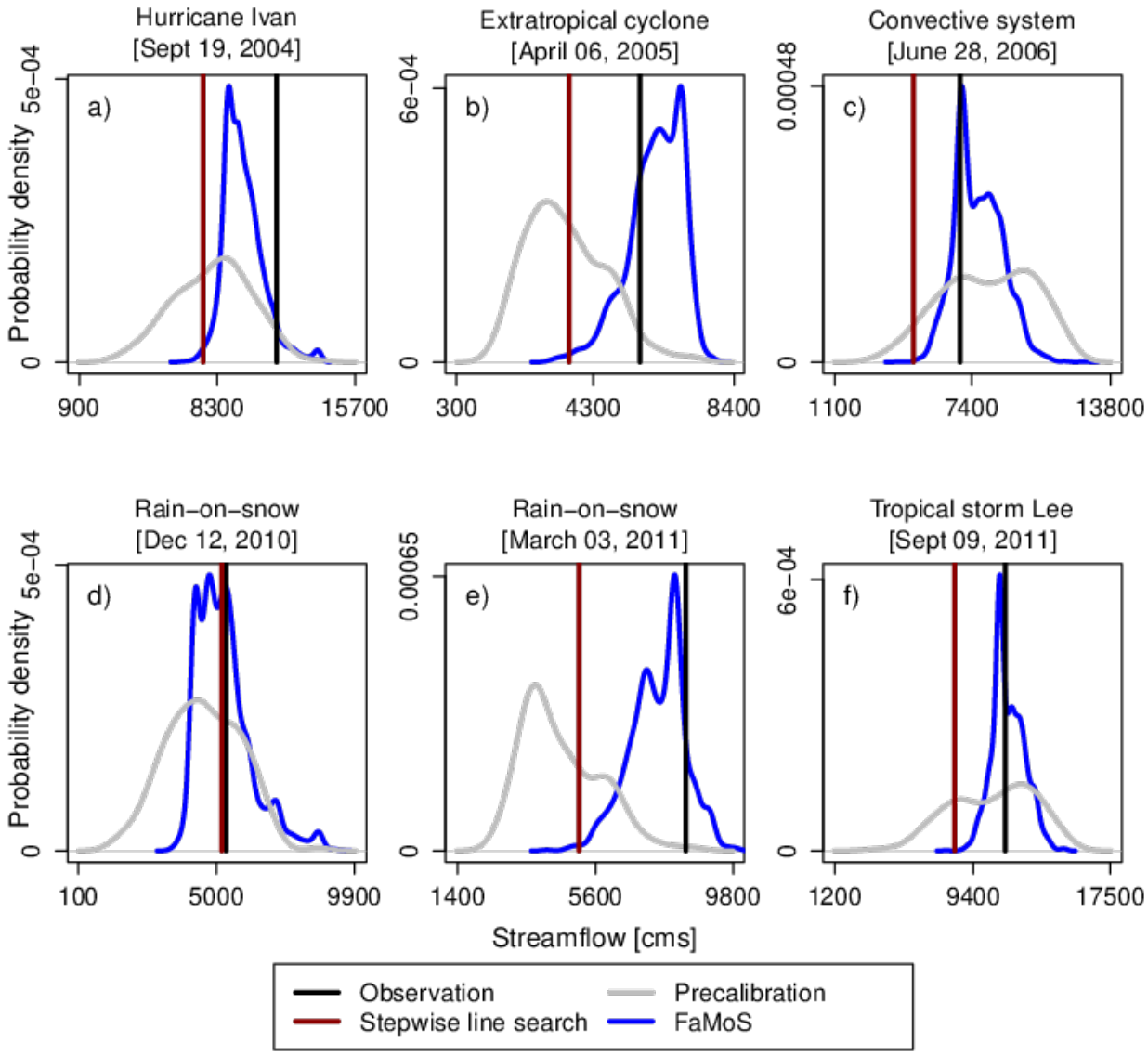

536

537 **Figure 4:** (a) - (c) Calibration and (d) - (f) and out-of-sample prediction for different flood events.

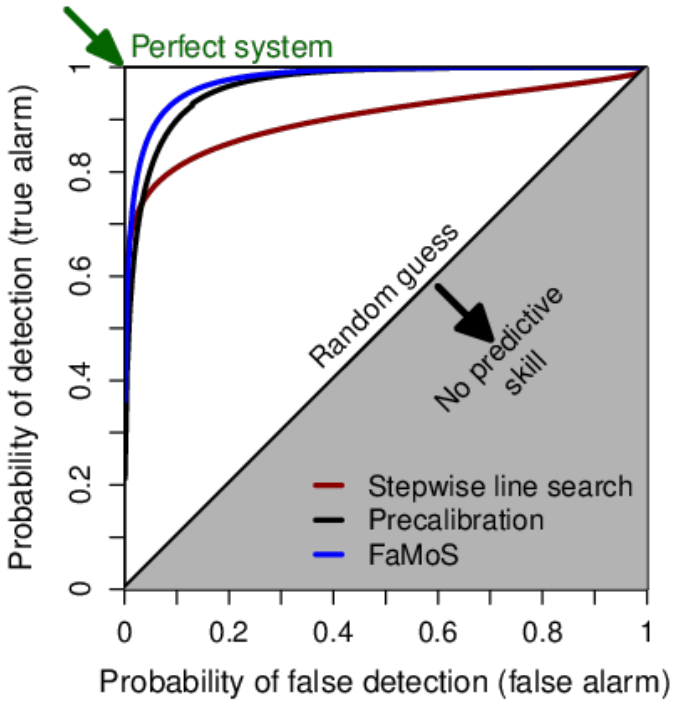

538

539

540 **Figure 5:** Relative operating characteristics (ROC) curve for different calibration approaches.
541 ROC curve plots the probability of detection against the probability of false detection for a range
542 of forecast probability levels. The ROC measures the trade-off between the fraction of ensemble
543 that correctly predict the occurrence of an event (probability of detection) and the fraction that
544 incorrectly predict its occurrence (probability of false detection). A larger area under the ROC
545 curve represents a more skillful prediction, with more ability to discriminate between flood
546 thresholds. The area under the ROC curve can range between 0 and 1, where a score of 1 implies
547 perfect discrimination and a score of 0.5 or less implies predictive discrimination that is no better
548 than a random guess. We also compute the ROC score. The ROC score measures the average gain
549 over climatology for all probability levels. The ROC score for stepwise line search, precalibration
550 and FAMOS is 0.55, 0.85 and 0.96 respectively.

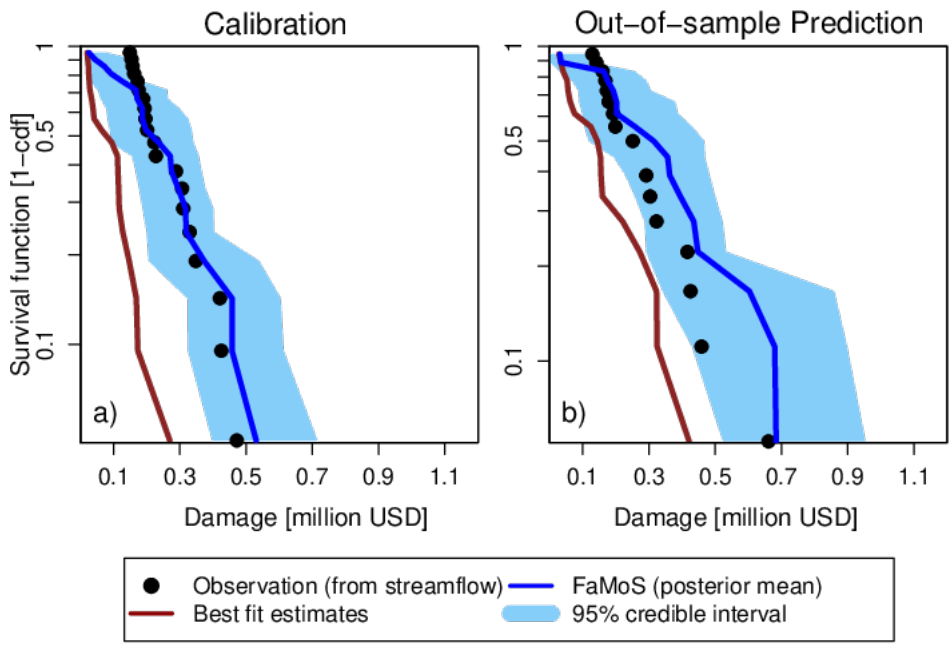

551

552 **Figure 6:** Survival function (one minus the cumulative frequency) for damage estimates using
553 streamflow obtained using the best parameter set (stepwise line search) and parameter distribution
554 (FaMoS). We show damage estimates for a) calibration and b) out-of-sample prediction. cdf=
555 cumulative distribution function.

Appendix A: Fast Model Calibrations (FaMoS) Details

1 Bayesian Calibration Framework

Suppose we have an observed time series $\mathbf{Z} = (Z(r_1), ..., Z(r_n))'$ times $r_i \in \mathcal{R}$ where $\mathcal{R}$ is the temporal domain of the process. We also have a deterministic computer model that generates a temporal process, or time series, at times $r_i \in \mathcal{R}$. Let $Y(r, \boldsymbol{\theta})$ be the computer model output at the time $r \in \mathcal{R}$ and the parameter (input) setting $\boldsymbol{\theta} \in \Theta \subseteq \mathbb{R}^d$. Θ is the parameter space of the computer model with integer d being the number of input parameters. In this study, we use a discontinuous temporal domain at R distinct time points $\nabla = (r_1, ..., r_R)'$. The vector $\mathbf{Y}(\boldsymbol{\theta}_i) = (Y(r_1, \boldsymbol{\theta}_i), ..., Y(r_R, \boldsymbol{\theta}_i))'$ is the computer model output corresponding to parameter setting $\boldsymbol{\theta}_i$. For input parameter setting $\boldsymbol{\theta}$, we model the observations $\mathbf{Z}$ as:

$$\mathbf{Z} = \mathbf{Y}(\boldsymbol{\theta}) + \boldsymbol{\delta} + \boldsymbol{\epsilon}, \tag{A1}$$

where $\boldsymbol{\epsilon} \sim N(\mathbf{0}, \sigma_\epsilon^2 \mathbf{I})$ are the independently and identically distributed observational error, and $\boldsymbol{\delta} \in \mathbb{R}^n$ is a systemic data-model discrepancy term, which can be modeled as a zero-mean Gaussian process (Bhat et al., 2010; Bayarri et al., 2007) or other flexible functional forms (Brynjarsdottir and O'Hagan, 2014).

In the Bayesian calibration framework, we obtain samples (via a Markov chain Monte Carlo (MCMC) algorithm) from the posterior distribution:

$$\tilde{\pi}(\boldsymbol{\theta}, \sigma_\epsilon^2, \boldsymbol{\delta}|\mathbf{Z}) \propto L(\boldsymbol{\theta}, \sigma_\epsilon^2, \boldsymbol{\delta}|\mathbf{Z})\pi(\boldsymbol{\theta})\pi(\sigma_\epsilon^2)\pi(\boldsymbol{\delta}), \tag{A2}$$

where $L(\boldsymbol{\theta}, \sigma_\epsilon^2, \boldsymbol{\delta}|\mathbf{Z})$ denotes the likelihood function and $\pi(\cdot)$ represents the prior distribution for the respective parameters and discrepancy term. Note that each evaluation of $L(\boldsymbol{\theta}, \sigma_\epsilon^2, \boldsymbol{\delta}|\mathbf{Z})$ requires running the computer model using specific input parameters $\boldsymbol{\theta}$. Hence, MCMC-based calibration approaches are sensible for computer models with shorter single model run walltimes, typically under 5 seconds per model run (Lee et al., 2020). For our study, we estimate that a standard MCMC-based calibration approach would on the order of years to approximate the posterior distribution $\tilde{\pi}(\boldsymbol{\theta}, \sigma_\epsilon^2, \boldsymbol{\delta}|\mathbf{Z})$. We estimated the time using the Metropolis-Hastings algorithm with an all-at-once update for the model parameters ($\boldsymbol{\theta}$). The dominating cost lies in evaluating the likelihood function, which requires running the hydrological model. For our case study, the HL-RDHM distributed hydrological model takes approximately 14.7 minutes per run on a single 2.3-GHz Intel Xeon E5-2697V4 (Broadwell) processor. Based on these values, 100,000 iterations of the all-at-once Metropolis-Hastings algorithm at 14.7 minutes per iteration would take 2.79 years of wall-time.

2 Particle-based Calibration Framework

We calibrate the HL-RDHM distributed hydrological model using the fast particle-based approach from Lee et al. (2020), which is built upon traditional Sequential Monte Carlo algorithms (Del Moral et al., 2006; Doucet et al., 2000; Liu and West, 2001), notably the Iterated Batch Importance Sampling (IBIS) (Chopin, 2002; Crisan and Doucet, 2000) method.

This method approximates the posterior distribution $\tilde{\pi}(\boldsymbol{\theta}, \sigma_\epsilon^2, \boldsymbol{\delta}|\mathbf{Z})$ using an evolving ensemble of particles.

We simplify the notation for an arbitrary target distribution as $\pi(\boldsymbol{\theta})$ with random variable $\boldsymbol{\theta} \in \mathbb{R}^d$. In the hydrological model calibration framework, the target distribution $\pi(\boldsymbol{\theta})$ would be the posterior distribution $\tilde{\pi}(\boldsymbol{\theta}, \sigma_\epsilon^2, \boldsymbol{\delta}|\mathbf{Z})$ with random variables $\boldsymbol{\theta}, \sigma_\epsilon^2$, and $\boldsymbol{\delta}$ and observations $\mathbf{Z}$. Suppose we want to estimate $\boldsymbol{\mu} = E_\pi\big[g(\boldsymbol{\theta})\big]$. Given $q(\boldsymbol{\theta}) > 0$ whenever $g(\boldsymbol{\theta})\pi(\boldsymbol{\theta}) > 0, \quad \forall \boldsymbol{\theta} \in \Theta$. Then $E_\pi\big[g(\boldsymbol{\theta})\big] = E_q\Big[g(\boldsymbol{\theta})w(\boldsymbol{\theta})\Big]$, where $w(\boldsymbol{\theta}) = \frac{\pi(\boldsymbol{\theta})}{q(\boldsymbol{\theta})}$ is the importance weight and $\sum_{i=1}^N w(\boldsymbol{\theta}_i) = 1$. The importance sampling estimator is $\hat{\boldsymbol{\mu}}_n = \frac{1}{n}\sum_{i=1}^N g(\boldsymbol{\theta}_i)w(\boldsymbol{\theta}_i)$ and $\hat{\boldsymbol{\mu}}_n \to \boldsymbol{\mu}$ with probability 1 as $n \to \infty$ by the strong law of large numbers. For target distributions with an unknown normalizing constant, the weights can be normalized as follows:

$$\tilde{w}(\boldsymbol{\theta}_i) = \frac{w(\boldsymbol{\theta}_i)}{\sum_{j=1}^n w(\boldsymbol{\theta}_j)} = \frac{\pi(\boldsymbol{\theta}_i)/q(\boldsymbol{\theta}_i)}{\sum_{j=1}^n w(\boldsymbol{\theta}_j)} \tag{A3}$$

where $\sum_{i=1}^N \tilde{w}(\boldsymbol{\theta}_i) = 1$.

Sampling-Importance-Resampling (Gordon et al., 1993; Doucet et al., 2001) approximates a target distribution $\pi(\boldsymbol{\theta})$ with an empirical distribution of the particles $\hat{\pi}(\boldsymbol{\theta})$ from an importance function $q(\boldsymbol{\theta})$ such as the prior distribution. The empirical distribution $\bar{\pi}(\boldsymbol{\theta})$ is defined as:

$$\bar{\pi}(\boldsymbol{\theta}) = \sum_{i=1}^N \tilde{w}(\boldsymbol{\theta}_i)\delta(\boldsymbol{\theta}_i) \approx \pi(\boldsymbol{\theta}), \tag{A4}$$

where $\tilde{w}(\boldsymbol{\theta}_i)$ are the normalized importance weights, $\delta(\boldsymbol{\theta}_i)$ is a Dirac measure that places unit mass at $\boldsymbol{\theta}_i$ and $\sum_{i=1}^N \tilde{w}(\boldsymbol{\theta}_i) = 1$.

Poor choices of importance functions can lead to inaccurate approximations of the target distribution (Doucet et al., 2000) where the bulk of the particles $\boldsymbol{\theta}_i$'s do not reside in the high-probability regions of the target distribution $\pi(\boldsymbol{\theta})$. Weight degeneracy occurs when the vast majority of the particles have near-zero importance weights. Multinomial resampling methods can combat weight degeneracy by eliminating the particles with very small important weights and replicating those with higher weights (Gordon et al., 1993; Doucet et al., 2000). After resampling, we reset all importance weights such that $w(\boldsymbol{\theta}_i) = 1/N$ and use the unweighted empirical distribution $\ddot{\pi}(\boldsymbol{\theta})$:

$$\ddot{\pi}(\boldsymbol{\theta}) = \frac{1}{N}\sum_{i=1}^N N_i\delta(\boldsymbol{\theta}_i), \tag{A5}$$

where N_i is the number of replicates corresponding to particle $\boldsymbol{\theta}_i$ and $\sum_{i=1}^N N_i = N$. Extreme weight degeneracy, where very few particles have any significant weight, can lead to sample impoverishment where a few unique particles $\boldsymbol{\theta}_i$'s are heavily replicated in the re-sampling step; hence, the empirical distribution $\ddot{\pi}(\boldsymbol{\theta})$ may poorly approximate the target distribution $\pi(\boldsymbol{\theta})$.

An alternative method mutates the replicated particles with samples from $K(\boldsymbol{\theta}_i^{(t-1)})$, the Metropolis-Hastings transition kernel (Gilks and Berzuini, 2001), whose stationary distribution is also the target distribution $\pi(\boldsymbol{\theta})$. The mutation stage proceeds with K Metropolis-Hastings updates for each particle $\boldsymbol{\theta}_i$, for $i = 1, ..., N$. Alternative mutation schemes use

genetic algorithms (Zhu et al., 2018) or different families of transition kernels, $K(\cdot)$ (Papaioannou et al., 2016; Murray et al., 2016). We set the K-th sample drawn via MCMC as the mutated particle $\tilde{\boldsymbol{\theta}}_i$. Since $\tilde{\boldsymbol{\theta}}_i \sim \pi(\boldsymbol{\theta})$, the resulting empirical distribution $\hat{\pi}(\boldsymbol{\theta})$ approximates the target distribution $\pi(\boldsymbol{\theta})$:

$$\pi(\boldsymbol{\theta}) \approx \hat{\pi}(\boldsymbol{\theta}) = \sum_{i=1}^{N} \tilde{\boldsymbol{\theta}}_i \delta(\tilde{\boldsymbol{\theta}}_i). \tag{A6}$$

Unfortunately, poor importance functions can result in severe sample impoverishment, which may require very long (and costly) mutation stages to provide an accurate representation of the target distribution (Li et al., 2014). Mixture approximations (Gordon et al., 1993) or kernel smoothing methods (Liu and West, 2001) can mutate or rejuvenate the replicated particles. However, these methods may not scale well to high-dimensional target distributions (Doucet et al., 2000).

2.1 Fast Particle-based Approach For Computer Model Calibration

In this study, we aim to approximate the posterior $\tilde{\pi}(\boldsymbol{\theta}, \boldsymbol{\delta}, \sigma_\epsilon^2|\mathbf{Z})$ from a computationally efficient approach. The fast particle-based approach (Lee et al., 2020) utilizes a set of tempered, or intermediate, posterior distributions $\tilde{\pi}_t(\boldsymbol{\theta}, \boldsymbol{\delta}, \sigma_\epsilon^2|\mathbf{Z})$ for $t = 1, ..., T$, which will act as both the importance functions and target distributions. Intermediate posterior distributions can be generated using likelihood tempering (Chopin, 2002; Neal, 2001; Liang and Wong, 2001) where the tth intermediate posterior distribution is defined as:

$$\tilde{\pi}_t(\boldsymbol{\theta}, \boldsymbol{\delta}, \sigma_\epsilon^2|\mathbf{Z}) \propto L(\boldsymbol{\theta}, \boldsymbol{\delta}, \sigma_\epsilon^2|\mathbf{Z})^{\gamma_t} \pi(\boldsymbol{\theta})\pi(\boldsymbol{\delta})\pi(\sigma_\epsilon^2), \tag{A7}$$

where γ_t's are determined according to a schedule where $\gamma_0 = 0 < \gamma_1 < \cdots < \gamma_T = 1$. For each $\tilde{\pi}_t(\boldsymbol{\theta}, \boldsymbol{\delta}, \sigma_\epsilon^2|\mathbf{Z})$, the likelihood component is a fractional power of the original likelihood $L(\boldsymbol{\theta}, \boldsymbol{\delta}, \sigma_\epsilon^2|\mathbf{Z})$. Using an adaptive incorporation schedule (Lee et al., 2020), we can select the appropriate $\boldsymbol{\gamma} = \{\gamma_0, \gamma_1, ..., \gamma_T\}$ within the calibration algorithm.

For cycle $t = 1$, we set the importance distribution to be the prior distribution $p(\boldsymbol{\theta}, \boldsymbol{\delta}, \sigma_\epsilon^2) = p(\boldsymbol{\theta})p(\boldsymbol{\delta})p(\sigma_\epsilon^2)$, and the target distribution to be the first intermediate posterior distribution, $\pi_1(\boldsymbol{\theta}, \boldsymbol{\delta}, \sigma_\epsilon^2|\mathbf{Z})$. For subsequent cycles t, the importance distribution is $\pi_{t-1}(\boldsymbol{\theta}, \boldsymbol{\delta}, \sigma_\epsilon^2|\mathbf{Z})$ and the target distribution is $\pi_t(\boldsymbol{\theta}, \boldsymbol{\delta}, \sigma_\epsilon^2|\mathbf{Z})$.

Next, we mutate the particles via short runs of the Metropolis-Hastings algorithm, where the stationary distribution is $\pi_t(\boldsymbol{\theta}, \boldsymbol{\delta}, \sigma_\epsilon^2|\mathbf{Z})$, the t-th intermediate posterior distribution. Note that the importance and target distributions are consecutive (t-th and (t+1)-th) intermediate posterior distributions, so there is considerable overlap between the high-probability regions of the two distributions. In the mutation stage, we employ the stopping rule from Lee et al. (2020) to control the number of Metropolis-Hastings updates; thereby preventing any unnecessary computer model runs. The mutation stages ends when the Bhattacharyya distance (Bhattacharyya, 1946) between two sets of particles from the mutation stage stablizes.

2.2 Adaptive incorporation schedule

To reduce computational costs and potentially reduce unnecessary computer model evaluations, we adopt the adaptive incorporation schedule from Lee et al. (2020). For avoid confusion, we simplify the notation in this subsection by defining $\tilde{\boldsymbol{\theta}} = (\boldsymbol{\theta}, \sigma_\epsilon^2, \boldsymbol{\delta})$, the combined vector of unknown parameters. Upon initialization, we set the first incorporation increment $\gamma_0 = 0$. We draw the initial set of particles $\tilde{\boldsymbol{\theta}}_0$ from $\tilde{\pi}_0(\tilde{\boldsymbol{\theta}}|\mathbf{Z}) \propto L(\tilde{\boldsymbol{\theta}}|\mathbf{Z})^0 \pi(\tilde{\boldsymbol{\theta}}) = \pi(\tilde{\boldsymbol{\theta}})$, the prior distribution of model parameters. For the subsequent cycles $t = 1, 2, 3, ...,$ we calculate the full likelihood $L(\tilde{\boldsymbol{\theta}}_{t-1}^{(i)}|\mathbf{Z})$ for $i = 1, ..., N$ where $\tilde{\boldsymbol{\theta}}_{t-1}^{(i)}$ denotes the parameter samples from the previous cycle $t-1$. Next, we compute the optimal γ_t that returns an effective sample size (ESS) of ESS_{thresh} or a sample size closest to ESS_{thresh}: $\gamma_t = \text{argmin}_\gamma\{(ESS_\gamma - ESS_{thresh})^2\}$, where $\gamma \in (\gamma_{min}, 1 - \gamma_{t-1})$, γ_{min} is a previously set minimum incorporation value, $ESS_{\gamma_t} = \sum_{i=1}^{N} 1/w_t(\tilde{\boldsymbol{\theta}}_t^{(i)})^2$, and $w_t(\tilde{\boldsymbol{\theta}}_t^{(i)}) \propto L(\tilde{\boldsymbol{\theta}}_t^{(i)}|\mathbf{Z})^\gamma$. Note that we can lower computational costs by evaluating the full likelihood $L(\tilde{\boldsymbol{\theta}}_t^{(i)}|\mathbf{Z})$ only once before the optimization.

We stop the scheduling algorithm when $\sum_{i=1}^{t} \gamma_t = 1$, or when the entire likelihood has been incorporated and the target distribution evolves to the full posterior distribution $\tilde{\pi}(\tilde{\boldsymbol{\theta}}|\mathbf{Z})$. Note at each cycle t, we set the incorporation increment (γ_t) to be between γ_{min} and $1 - \sum_{i=1}^{t} \gamma_t$. The user will typically set the minimum incorporation increment γ_{min} and the threshold effective sample size, ESS_{thresh}. We provide our choice of γ_{min} and ESS_{thresh} in the next section (Implementation Details).

Adaptive likelihood incorporation schedule

1. Initialization: At $t = 0$, set $\gamma_0 = 0$.
2. When $t > 0$ and $\sum_{i=1}^{t-1} \gamma_i < 1$
   - Compute $L(\tilde{\boldsymbol{\theta}}_{t-1}^{(i)}|\mathbf{Z})$ for $i = 1, ..., N$
   - Set $\gamma_t = \text{argmin}_\gamma\{(ESS_\gamma - ESS_{thresh})^2\}$, where $ESS_\gamma = \sum_{i=1}^{N} \frac{1}{w_t^{(i)2}}$, $w_t^{(i)} \propto L(\tilde{\boldsymbol{\theta}}_t^{(i)}|\mathbf{Z})^\gamma$, and $\gamma \in (\gamma_{min}, 1 - \gamma_{t-1})$.
   - Update $t \leftarrow t + 1$
3. When $\sum_{i=1}^{t-1} \gamma_i = 1$: Stop Calibration

2.3 HL-RDHM Calibration: Implementation Details

We now return to the original notation of the unknown parameters $\boldsymbol{\theta}, \sigma_\delta^2$, and σ_ϵ^2. The target distribution is the full posterior distribution $\tilde{\pi}(\boldsymbol{\theta}, \sigma_\delta^2, \sigma_\epsilon^2|\mathbf{Z})$ and the Bayesian hierarchical framework for the HL-RDHM distributed hydrological model calibration is as follows:

$$\text{Data Model:} \quad \mathbf{Z}|\mathbf{Y}(\cdot), \boldsymbol{\theta}, \boldsymbol{\delta}, \sigma_\epsilon^2 \sim \mathcal{N}(\mathbf{Y}(\boldsymbol{\theta}) + \boldsymbol{\delta}, \sigma_\epsilon^2 \mathcal{I}) \tag{A8}$$

$$\text{Process Model:} \quad \boldsymbol{\delta}|\sigma_\delta^2 \sim \mathcal{N}(\mathbf{0}, \sigma_\delta^2 \mathcal{I}) \tag{A9}$$

$$\text{Parameter Model:} \quad \boldsymbol{\theta} \sim \pi(\boldsymbol{\theta}), \quad \sigma_\delta^2 \sim \pi(\sigma_\delta^2), \quad \sigma_\epsilon^2 \sim \pi(\sigma_\epsilon^2) \tag{A10}$$

Algorithm 1: Fast Particle-based Calibration

Data: Z

Initialization:

Draw $\tilde{\boldsymbol{\theta}}_0^{(i)} \sim p(\tilde{\boldsymbol{\theta}})$ for particles $i = 1, ..., N$.

Set $w_0^{(i)} = 1/N$, $\gamma_0 = 0$, and K;

for *cycles* $t = 1, ..., T$ **do**

1. Compute full likelihood:

Calculate $L(\tilde{\boldsymbol{\theta}}_{t-1}^{(i)}|\mathbf{Z})$ for $i = 1, ..., N$;

2. Select optimal likelihood incorporation increment γ_t:

Set $\gamma_t = \text{argmin}_\gamma\{(ESS_{\gamma_t} - ESS_{thresh})^2\}$, where $\gamma \in (0.1, 1 - \sum_{h=1}^{t-1} \gamma_h)$

Note: $ESS_{\gamma_t} = \sum_{i=1}^{N} \frac{1}{w_t^{(i)2}}$ and $w_t^{(i)} \propto L(\tilde{\boldsymbol{\theta}}_t^{(i)}|\mathbf{Z})^{\gamma_t}$;

3. Compute importance weights:

$w_t^{(i)} \propto w_{t-1}^{(i)} \times L(\tilde{\boldsymbol{\theta}}_t^{(i)}|\mathbf{Z})^{\gamma_t}$;

4. Re-sample particles via multinomial sampling:

Draw $\tilde{\boldsymbol{\theta}}_t^{(i)}$ from $\{\tilde{\boldsymbol{\theta}}_{t-1}^{(1)}, ..., \tilde{\boldsymbol{\theta}}_{t-1}^{(N)}\}$ with probabilities $\propto \{w_t^{(1)}, ..., w_t^{(N)}\}$;

5. Set intermediate posterior distribution:

Set $\pi_t(\tilde{\boldsymbol{\theta}}|\mathbf{Z}) \propto L(\tilde{\boldsymbol{\theta}}_i|\mathbf{Z})^{\tilde{\gamma}}\pi(\tilde{\boldsymbol{\theta}})$, where $\tilde{\gamma} = \sum_{j=1}^{t} \gamma_j$;

6. Mutation:

Using each particle $(\tilde{\boldsymbol{\theta}}_t^{(1)}, ..., \tilde{\boldsymbol{\theta}}_t^{(N)})$ as the initial value, run N chains of an MCMC algorithm with target distribution $\pi_t(\tilde{\boldsymbol{\theta}}|Z)$ for $2K$ iterations

7. Check stopping criterion:

Compute $\delta_B = D_B(h(\tilde{\boldsymbol{\theta}}_t^K), h(\tilde{\boldsymbol{\theta}}_t^{2K}))$;

if $\delta_B < \epsilon_B$ **then**

Set $\tilde{\boldsymbol{\theta}}_t^{(i)} = \tilde{\boldsymbol{\theta}}_t^{(i),2K}$;

else

Run K additional updates and re-evaluate stopping criterion

Continue until stopping criterion is met

8. Stop when full likelihood is incorporated;

if $\sum_{i=1}^{N} \gamma_t = 1$ **then**

End Algorithm;

else

Reset weights: $w_t^{(i)} = 1/N$ for particles $i = 1, ..., N$;

Set t=t+1 and return to Step 1;

where $\pi(\boldsymbol{\theta})$, $\pi(\sigma_\delta^2)$, and $\pi(\sigma_\epsilon^2)$ denote the prior distributions of $\boldsymbol{\theta}$, σ_δ^2, and σ_ϵ^2, respectively. For $\pi(\boldsymbol{\theta})$, we place a priori independent uniform priors on each of the model parameters with ranges (lower and upper bounds) based on domain-area expertise.

Instead of estimating the nuisance parameters σ_δ^2 and σ_ϵ^2 separately, we chose to combine these as $\sigma^2 = \sigma_\delta^2 + \sigma_\epsilon^2$. We place a standard non-informative inverse gamma prior on the combined error variance $\sigma_\epsilon^2 \sim IG(0.2, 0.2)$. Note that we assume conditional independence among the extreme observations given the model outputs. The updated Bayesian hierarchical framework is:

$$\text{Data Model:} \qquad \mathbf{Z}|\mathbf{Y}(\cdot), \boldsymbol{\theta}, \sigma^2 \sim \mathcal{N}(\mathbf{Y}(\boldsymbol{\theta}), \sigma^2 \mathcal{I}) \tag{A11}$$

$$\text{Parameter Model:} \qquad \boldsymbol{\theta} \sim \pi(\boldsymbol{\theta}), \quad \sigma^2 \sim \pi(\sigma^2) \tag{A12}$$

While much of the fast particle-based approach is automated, the user must select the: (1) total number of particles, N; (2) baseline number of Metropolis-Hastings updates run before checking the stopping criterion, K; (3) minimum incorporation γ_{min} at each cycle; and (4) the effective sample size threshold ESS_{thresh}. We chose $N = 2015$ particles based on the available resources. On the Cheyenne HPC, this requires 56 nodes with 36 processors per node. For the stopping criterion, we use $K = 7$ as the baseline length. The floor for the incorporation increment is fixed at $\gamma_{min} = 0.1$ such that we incoporate at least $L(\boldsymbol{\theta}|\mathbf{Z})^{0.1}$ into the intermediate posterior at each cycle. Finally, the $ESS_{thresh} = N/2$, which is the typical threshold that activates resampling in many sequential Monte Carlo methods (Del Moral et al., 2006).We calibrate the HL-RDHM distributed hydrological model using Cheyenne (Computational and Information Systems Laboratory, 2017), a 5.34-petaflops high performance computer operated by the National Center for Atmospheric Research (NCAR). We employ message passing interface (MPI) and the `R` package `Rmpi` for any parallelized operations such as computing importance weights and particle mutation.

Consider the vector of HL-RDHM model parameters $\boldsymbol{\theta} = (\theta_1, ..., \theta_{12})'$. The prior distribution $\pi(\theta_j)$ for the j-th model parameters follow a univariate uniform distribution with lower and upper bounds specified by our hydrological model experts. $\theta_j \sim Unif(l_j, u_j)$ with hyperparameters l_j(lower bound) and u_j (upper bound) specified in Table S1. We place a standard non-informative inverse gamma prior on the combined error variance $\sigma^2 \sim IG(\alpha_{\sigma^2}, \beta_{\sigma^2})$ where $\alpha_{\sigma^2} = 0.2$ and $\beta_{\sigma^2} = 0.2$.

References

Bayarri, M., Berger, J., Cafeo, J., Garcia-Donato, G., Liu, F., Palomo, J., Parthasarathy, R., Paulo, R., Sacks, J., Walsh, D., et al. (2007). Computer model validation with functional output. *The Annals of Statistics*, 35(5):1874–1906.

Bhat, K. S., Haran, M., Goes, M., and Chen, M. (2010). Computer model calibration with multivariate spatial output: A case study. *Frontiers of Statistical Decision Making and Bayesian Analysis*, pages 168–184.

Bhattacharyya, A. (1946). On a measure of divergence between two multinomial populations. *Sankhyā: The Indian Journal of Statistics*, pages 401–406.

Brynjarsdottir, J. and O'Hagan, A. (2014). Learning about physical parameters: The importance of model discrepancy. *Inverse Problems*, 30(11):114007.

Chopin, N. (2002). A sequential particle filter method for static models. *Biometrika*, 89(3):539–552.

Computational and Information Systems Laboratory (2017). Cheyenne: HPE/SGI ICE XA System (University Community Computing). Boulder, CO: National Center for Atmospheric Research. doi:10.5065/D6RX99HX.

Crisan, D. and Doucet, A. (2000). Convergence of sequential Monte Carlo methods. *Signal Processing Group, Department of Engineering, University of Cambridge, Technical Report CUED/F-INFENG/TR381*, 1.

Del Moral, P., Doucet, A., and Jasra, A. (2006). Sequential Monte Carlo samplers. *Journal of the Royal Statistical Society: Series B*, 68(3):411–436.

Doucet, A., De Freitas, N., and Gordon, N. (2001). An introduction to sequential Monte Carlo methods. In *Sequential Monte Carlo Methods in Practice*, pages 3–14. Springer.

Doucet, A., Godsill, S., and Andrieu, C. (2000). On sequential Monte Carlo sampling methods for Bayesian filtering. *Statistics and Computing*, 10(3):197–208.

Gilks, W. R. and Berzuini, C. (2001). Following a moving target—Monte Carlo inference for dynamic Bayesian models. *Journal of the Royal Statistical Society: Series B (Statistical Methodology)*, 63(1):127–146.

Gordon, N. J., Salmond, D. J., and Smith, A. F. (1993). Novel approach to nonlinear/non-Gaussian Bayesian state estimation. In *IEE Proceedings F-radar and Signal Processing*, volume 140, pages 107–113. IET.

Lee, B. S., Haran, M., Fuller, R. W., Pollard, D., and Keller, K. (2020). A fast particle-based approach for calibrating a 3-d model of the antarctic ice sheet. *The Annals of Applied Statistics*, 14(2):605–634.

Li, T., Sun, S., Sattar, T. P., and Corchado, J. M. (2014). Fight sample degeneracy and impoverishment in particle filters: A review of intelligent approaches. *Expert Systems with Applications*, 41(8):3944–3954.

Liang, F. and Wong, W. H. (2001). Real-Parameter Evolutionary Monte Carlo with applications to Bayesian mixture models. *Journal of the American Statistical Association*, 96(454):653–666.

Liu, J. and West, M. (2001). Combined parameter and state estimation in simulation-based filtering. In *Sequential Monte Carlo Methods in Practice*, pages 197–223. Springer.

Murray, L. M., Lee, A., and Jacob, P. E. (2016). Parallel resampling in the particle filter. *Journal of Computational and Graphical Statistics*, 25(3):789–805.

Neal, R. M. (2001). Annealed importance sampling. *Statistics and Computing*, 11(2):125–139.

Papaioannou, I., Papadimitriou, C., and Straub, D. (2016). Sequential importance sampling for structural reliability analysis. *Structural Safety*, 62:66–75.

Zhu, G., Li, X., Ma, J., Wang, Y., Liu, S., Huang, C., Zhang, K., and Hu, X. (2018). A new moving strategy for the sequential Monte Carlo approach in optimizing the hydrological model parameters. *Advances in Water Resources*, 114:164–179.

References

Alfieri, L., Bisselink, B., Dottori, F., Naumann, G., de Roo, A., Salamon, P., et al. (2017). Global projections of river flood risk in a warmer world. *Earth's Future*. https://doi.org/10.1002/2016ef000485

Anderson, R. M., Koren, V. I., & Reed, S. M. (2006). Using SSURGO data to improve Sacramento Model a priori parameter estimates. *Journal of Hydrology*, *320*(1), 103–116.

Asher, M. J., Croke, B. F. W., Jakeman, A. J., & Peeters, L. J. M. (2015). A review of surrogate models and their application to groundwater modeling. *Water Resources Research*. https://doi.org/10.1002/2015wr016967

Ashley, S. T., & Ashley, W. S. (2008). Flood Fatalities in the United States. *Journal of Applied Meteorology and Climatology*, *47*(3), 805–818.

Bain, A., & Crisan, D. (2008). *Fundamentals of Stochastic Filtering*. Springer Science & Business Media.

Bates, P. D., Quinn, N., Sampson, C., Smith, A., Wing, O., Sosa, J., et al. (2021). Combined modeling of US fluvial, pluvial, and coastal flood hazard under current and future climates. *Water Resources Research*, *57*(2). https://doi.org/10.1029/2020wr028673

Bayarri, M. J., Berger, J. O., Paulo, R., Sacks, J., Cafeo, J. A., Cavendish, J., et al. (2007a). A Framework for Validation of Computer Models. *Technometrics: A Journal of Statistics for the Physical, Chemical, and Engineering Sciences*, *49*(2), 138–154.

Bayarri, M. J., Walsh, D., Berger, J. O., Cafeo, J., Garcia-Donato, G., Liu, F., et al. (2007b). Computer model validation with functional output. *The Annals of Statistics*, *35*(5), 1874–1906.

Beven, K. J., and A. M. Binley, The future of distributed models: Model calibration and

uncertainty prediction, Hydrol. Processes, 6, 279–298, 1992.

Beven, K. (2014). The GLUE Methodology for Model Calibration with Uncertainty. *Applied Uncertainty Analysis for Flood Risk Management*. https://doi.org/10.1142/9781848162716_0006

Bhat, K. S., Haran, M., Goes, M., & Chen, M. (2010). Computer model calibration with multivariate spatial output: A case study. *Frontiers of Statistical Decision Making and Bayesian Analysis*, 168–184.

Bhattacharyya, A. (1946). On a Measure of Divergence between Two Multinomial Populations. *Journal of the Indian Society of Agricultural Statistics. Indian Society of Agricultural Statistics*, *7*(4), 401–406.

Bitew, M. M., & Gebremichael, M. (2011). Evaluation of satellite rainfall products through hydrologic simulation in a fully distributed hydrologic model. *Water Resources Research*, *47*(6). https://doi.org/10.1029/2010wr009917

Blasone, R.-S., J. A. Vrugt, H. Madsen, D. Rosbjerg, B. A. Robinson, and G. A. Zyvoloski (2008a), Generalized likelihood uncertainty estimation (GLUE) using adaptive Markov chain Monte Carlo sampling, Adv. Water Resour., 31, 630–648.

Boulange, J., Hanasaki, N., Yamazaki, D., & Pokhrel, Y. (2021). Role of dams in reducing global flood exposure under climate change. *Nature Communications*, *12*(1), 417.

Bowman, A. L., Franz, K. J., & Hogue, T. S. (2017). Case Studies of a MODIS-Based Potential Evapotranspiration Input to the Sacramento Soil Moisture Accounting Model. *Journal of Hydrometeorology*, *18*(1), 151–158.

Braak, C. J. F. T. (2006). A Markov Chain Monte Carlo version of the genetic algorithm Differential Evolution: easy Bayesian computing for real parameter spaces. *Statistics and*

Computing, *16*(3), 239–249.

Brunner, G. W. (1995). *HEC-RAS River Analysis System. Hydraulic Reference Manual. Version 1.0*. Hydrologic Engineering Center Davis CA. Retrieved from https://apps.dtic.mil/sti/citations/ADA311952

Brynjarsdóttir, J., & O'Hagan, A. (2014). Learning about physical parameters: the importance of model discrepancy. *Inverse Problems*, *30*(11), 114007.

Carlberg, B., Franz, K., & Gallus, W. (2020). A Method to Account for QPF Spatial Displacement Errors in Short-Term Ensemble Streamflow Forecasting. *WATER*, *12*(12), 3505.

Chang, W., Haran, M., Olson, R., & Keller, K. (2014). Fast dimension-reduced climate model calibration and the effect of data aggregation. *The Annals of Applied Statistics*, *8*(2), 649–673.

Chang, W., Haran, M., Applegate, P., & Pollard, D. (2016). Calibrating an Ice Sheet Model Using High-Dimensional Binary Spatial Data. *Journal of the American Statistical Association*, *111*(513), 57–72.

Chester, M. V., Shane Underwood, B., & Samaras, C. (2020). Keeping infrastructure reliable under climate uncertainty. *Nature Climate Change*. https://doi.org/10.1038/s41558-020-0741-0

Chopin, N. (2002). A sequential particle filter method for static models. *Biometrika*, *89*(3), 539–552.

Computational and Information Systems Laboratory (2017). Cheyenne: HPE/SGI ICE XA System (University Community Computing). Boulder, CO: National Center for Atmospheric Research. doi:10.5065/D6RX99HX.

Constantine, P. G., Dow, E., & Wang, Q. (2014). Active Subspace Methods in Theory and Practice: Applications to Kriging Surfaces. *SIAM Journal on Scientific Computing*. https://doi.org/10.1137/130916138

Coulthard, T. J., Neal, J. C., Bates, P. D., Ramirez, J., de Almeida, G. A. M., & Hancock, G. R. (2013). Integrating the LISFLOOD-FP 2D hydrodynamic model with the CAESAR model: implications for modelling landscape evolution. *Earth Surface Processes and Landforms*, *38*(15), 1897–1906.

Craig, P. S., Goldstein, M., Seheult, A. H., & Smith, J. A. (1997). Pressure Matching for Hydrocarbon Reservoirs: A Case Study in the Use of Bayes Linear Strategies for Large Computer Experiments. In *Case Studies in Bayesian Statistics* (pp. 37–93). Springer New York.

Crisan, D., & Doucet, A. (2000). Convergence of sequential Monte Carlo methods. *Signal Processing Group, Department of Engineering, University of Cambridge, Technical Report CUEDIF-INFENGrrR38*, *1*. Retrieved from http://citeseerx.ist.psu.edu/viewdoc/download?doi=10.1.1.361.3193&rep=rep1&type=pdf

Davis and Skaggs. (1992). *Catalog of Residential Depth-Damage Functions Used by the Army Corps of Engineers in Flood Damage Estimation*. Retrieved from https://apps.dtic.mil/dtic/tr/fulltext/u2/a255462.pdf

Del Moral, P., Doucet, A., & Jasra, A. (2006). Sequential Monte Carlo samplers. Journal of the Royal Statistical Society: Series B, 68(3):411– 436.

Didier, D., Baudry, J., Bernatchez, P., Dumont, D., Sadegh, M., Bismuth, E., et al. (2019). Multihazard simulation for coastal flood mapping: Bathtub versus numerical modelling in an open estuary, Eastern Canada. *Journal of Flood Risk Management*, *12*(S1), e12505.

Doucet, A., Godsill, S., & Andrieu, C. (2000). *Statistics and Computing*, *10*(3), 197–208.

Doucet, A., de Freitas, N., & Gordon, N. (2001). An Introduction to Sequential Monte Carlo Methods. In A. Doucet, N. de Freitas, & N. Gordon (Eds.), *Sequential Monte Carlo Methods in Practice* (pp. 3–14). New York, NY: Springer New York.

Duan, Q., S. Sorooshian, and V. K. Gupta (1992), Effective and efficient global optimization for conceptual rainfall-runoff models, Water Resour. Res., 28(4), 1015–1031, doi:10.1029/91WR02985.

Edwards, N. R., Cameron, D., & Rougier, J. (2011). Precalibrating an intermediate complexity climate model. *Climate Dynamics*, *37*(7-8), 1469–1482.

Edwards, T. L., Brandon, M. A., Durand, G., Edwards, N. R., Golledge, N. R., Holden, P. B., Nias, I. J., Payne, A. J., Ritz, C., & Wernecke, A. (2019). Revisiting Antarctic ice loss due to marine ice-cliff instability, Nature, 566, 58–64, https://doi.org/10.1038/s41586-019-0901-4, 2019.

Fares, A., Awal, R., Michaud, J., Chu, P.-S., Fares, S., Kodama, K., & Rosener, M. (2014). Rainfall-runoff modeling in a flashy tropical watershed using the distributed HL-RDHM model. *Journal of Hydrology*, *519*, 3436–3447.

FEMA, 2019: Flood Insurance Rate Map (FIRM). Federal Emergency Management Agency, https://www.fema.gov/flood-insurance-ratemap-firm.

Fereshtehpour, M., & Karamouz, M. (2018). DEM resolution effects on coastal flood vulnerability assessment: Deterministic and probabilistic approach. *Water Resources Research*, *54*(7), 4965–4982.

Fisher, R. A., & Koven, C. D. (2020). Perspectives on the future of land surface models and the challenges of representing complex terrestrial systems. *Journal of Advances in Modeling*

Earth Systems, *12*(4). https://doi.org/10.1029/2018ms001453

Gilks, W. R., & Berzuini, C. (2001). Following a moving target-Monte Carlo inference for dynamic Bayesian models. *Journal of the Royal Statistical Society. Series B, Statistical Methodology*, *63*(1), 127–146.

Gomez, M., Sharma, S., Reed, S., & Mejia, A. (2019). Skill of ensemble flood inundation forecasts at short- to medium-range timescales. *Journal of Hydrology*, *568*, 207–220.

Goodman, J., & Weare, J. (2010). Ensemble samplers with affine invariance. *Communications in Applied Mathematics and Computational Science*, *5*(1), 65–80.

Gordon, N. J., Salmond, D. J., & Smith, A. F. M. (1993). Novel approach to nonlinear/non-Gaussian Bayesian state estimation. In *IEE Proceedings F-radar and signal processing* (Vol. 140, pp. 107–113). IET.

Gou, J., Miao, C., Duan, Q., Tang, Q., Di, Z., Liao, W., et al. (2020). Sensitivity Analysis-Based Automatic Parameter Calibration of the VIC Model for Streamflow Simulations Over China. *Water Resources Research*. https://doi.org/10.1029/2019wr025968

Gramacy, R. B. (2020). *Surrogates: Gaussian process modeling, design, and optimization for the applied sciences*. Chapman and Hall/CRC.

Gramacy, R. B., & Apley, D. W. (2015). Local Gaussian Process Approximation for Large Computer Experiments. *Journal of Computational and Graphical Statistics: A Joint Publication of American Statistical Association, Institute of Mathematical Statistics, Interface Foundation of North America*, *24*(2), 561–578.

Gupta, H. V., S. Sorooshian, and P. O. Yapo (1998), Toward improved calibration of hydrologic models: Multiple and noncommensurable measures of information, Water Resour. Res., 34(4), 751–763, doi:10.1029/97WR03495.

Gupta, H. V., Clark, M. P., Vrugt, J. A., Abramowitz, G., & Ye, M. (2012). Towards a comprehensive assessment of model structural adequacy. Water Resources Research, 48(8). https://doi.org/10.1029/2011WR011044

Helton, J. C., & Davis, F. J. (2003). Latin hypercube sampling and the propagation of uncertainty in analyses of complex systems. *Reliability Engineering & System Safety*, *81*(1), 23–69.

Herman, J. D., Reed, P. M., & Wagener, T. (2013). Time-varying sensitivity analysis clarifies the effects of watershed model formulation on model behavior. *Water Resources Research*, *49*(3), 1400–1414.

Higdon, D. (2003). for inference in computationally intensive inverse problems. In *Bayesian Statistics 7: Proceedings of the Seventh Valencia International Meeting* (p. 181). Oxford University Press.

Higdon, D., Kennedy, M., Cavendish, J. C., Cafeo, J. A., & Ryne, R. D. (2004). Combining Field Data and Computer Simulations for Calibration and Prediction. *SIAM Journal of Scientific Computing*, *26*(2), 448–466.

Higdon, D., Gattiker, J., Williams, B., & Rightley, M. (2008). Computer Model Calibration Using High-Dimensional Output. *Journal of the American Statistical Association*, *103*(482), 570–583.

Holden, P. B., Edwards, N. R., Oliver, K. I. C., Lenton, T. M., & Wilkinson, R. D. (2010). A probabilistic calibration of climate sensitivity and terrestrial carbon change in GENIE-1. *Climate Dynamics*, *35*(5), 785–806.

Homer, C., Dewitz, J., Yang, L., Jin, S., Danielson, P., Xian, G., et al. (2015). Completion of the 2011 National Land Cover Database for the conterminous United States--representing a decade of land cover change information. *Photogrammetric Engineering & Remote Sensing*,

81(5), 345–354.

Hsu, K.-L., Moradkhani, H., & Sorooshian, S. (2009). A sequential Bayesian approach for hydrologic model selection and prediction. *Water Resources Research*, *45*(12). https://doi.org/10.1029/2008wr006824

Hu, J., Chen, S., Behrangi, A., & Yuan, H. (2019). Parametric uncertainty assessment in hydrological modeling using the generalized polynomial chaos expansion. *Journal of Hydrology*, *579*, 124158.

Hwang, J. T., & Martins, J. R. R. A. (2018). A fast-prediction surrogate model for large datasets. *Aerospace Science and Technology*, *75*, 74–87.

Jeremiah, E., Sisson, S., Marshall, L., Mehrotra, R., & Sharma, A. (2011). Bayesian calibration and uncertainty analysis of hydrological models: A comparison of adaptive Metropolis and sequential Monte Carlo samplers. *Water Resources Research*, *47*(7). https://doi.org/10.1029/2010wr010217

Judi, D. R., Rakowski, C. L., Waichler, S. R., Feng, Y., & Wigmosta, M. S. (2018). Integrated Modeling Approach for the Development of Climate-Informed, Actionable Information. *WATER*, *10*(6), 775.

Kalyanaraman, J., Kawajiri, Y., Lively, R. P., & Realff, M. J. (2016). Uncertainty quantification via bayesian inference using sequential monte carlo methods for CO2adsorption process. *AIChE Journal*. https://doi.org/10.1002/aic.15381

Kamali, B., Mousavi, S. J., & Abbaspour, K. C. (2013). Automatic calibration of HEC-HMS using single-objective and multi-objective PSO algorithms. *Hydrological Processes*, *27*(26), 4028–4042.

Kantas, N., Beskos, A., & Jasra, A. (2014). Sequential Monte Carlo Methods for High-

Dimensional Inverse Problems: A Case Study for the Navier--Stokes Equations. *SIAM/ASA Journal on Uncertainty Quantification*, *2*(1), 464–489.

Kavetski, D., Kuczera, G., & Franks, S. W. (2006). Bayesian analysis of input uncertainty in hydrological modeling: 2. Application. Water resources research, 42(3). 10.1029/2005WR004376

Kavetski, D., Fenicia, F., Reichert, P., & Albert, C. (2018). Signature-Domain Calibration of Hydrological Models Using Approximate Bayesian Computation: Theory and Comparison to Existing Applications. *Water Resources Research*. https://doi.org/10.1002/2017wr020528

Kennedy, M. C., & O'Hagan, A. (2001). Bayesian calibration of computer models. *Journal of the Royal Statistical Society. Series B, Statistical Methodology*, *63*(3), 425–464.

Kim S, Shen H, Noh S, Seo DJ, Philips B (2021) High-resolution modeling and prediction of urban floods using WRF-Hydro and data assimilation. J Hydrol 598:1–14

Knutti, R., T. F. Stocker, F. Joos, and G.-K. Plattner (2002), Constraints on radiative forcing and future climate change from observations and climate model ensembles, Nature, 416, 719–723.

Koren, V., Reed, S., Smith, M., Zhang, Z., & Seo, D.-J. (2004). Hydrology laboratory research modeling system (HL-RMS) of the US national weather service. *Journal of Hydrology*, *291*(3), 297–318.

Kuzmin, V., Seo, D.-J., & Koren, V. (2008). Fast and efficient optimization of hydrologic model parameters using a priori estimates and stepwise line search. *Journal of Hydrology*, *353*(1), 109–128.

Lahmers, T. M., Hazenberg, P., Gupta, H., Castro, C., Gochis, D., Dugger, A., et al. (2021). Evaluation of NOAA National Water Model Parameter Calibration in Semiarid

Environments Prone to Channel Infiltration. *Journal of Hydrometeorology*, *22*(11), 2939–2969.

Lataniotis, C., Marelli, S., & Sudret, B. (2020). EXTENDING CLASSICAL SURROGATE MODELING TO HIGH DIMENSIONS THROUGH SUPERVISED DIMENSIONALITY REDUCTION: A DATA-DRIVEN APPROACH. *International Journal for Uncertainty Quantification*, *10*(1). https://doi.org/10.1615/Int.J.UncertaintyQuantification.2020031935

Laloy, E., & Vrugt, J. A. (2012). High-dimensional posterior exploration of hydrologic models using multiple-try DREAM(ZS) and high-performance computing. Water Resources Research, 48, W01526. https://doi.org/10.1029/2011WR010608

Lee, B. S., Haran, M., Fuller, R. W., Pollard, D., & Keller, K. (2020). A fast particle-based approach for calibrating a 3-D model of the Antarctic ice sheet. *The Annals of Applied Statistics*, *14*(2), 605–634.

Lempert, R. J. (2002). A new decision sciences for complex systems. *Proceedings of the National Academy of Sciences of the United States of America*, *99 Suppl 3*, 7309–7313.

Li, T., Sun, S., Sattar, T. P., & Corchado, J. M. (2014). Fight sample degeneracy and impoverishment in particle filters: A review of intelligent approaches. *Expert Systems with Applications*, *41*(8), 3944–3954.

Li, L., Shen, M., Hou, Y., Xu, C. Y., Lutz, A. F., Chen, J., … Chen, H. (2019). Twenty-first-century glacio-hydrological changes in the Himalayan headwater Beas River basin. Hydrology and Earth System Sciences, 23(3), 1483–1503. https://doi.org/10.5194/hess-23-1483-2019

Liang, F., & Wong, W. H. (2001). Real-Parameter Evolutionary Monte Carlo With Applications to Bayesian Mixture Models. *Journal of the American Statistical Association*, *96*(454), 653–

666.

Liu, J., & West, M. (2001). Combined Parameter and State Estimation in Simulation-Based Filtering. In A. Doucet, N. de Freitas, & N. Gordon (Eds.), *Sequential Monte Carlo Methods in Practice* (pp. 197–223). New York, NY: Springer New York.

Liu, J. S., Liang, F., & Wong, W. H. (2000). The Multiple-Try Method and Local Optimization in Metropolis Sampling. *Journal of the American Statistical Association*, *95*(449), 121–134.

Liu, X., & Guillas, S. (2017). Dimension Reduction for Gaussian Process Emulation: An Application to the Influence of Bathymetry on Tsunami Heights. *SIAM/ASA Journal on Uncertainty Quantification*, *5*(1), 787–812.

Liu, Y., Hejazi, M., Li, H., Zhang, X., & Leng, G. (2018). A hydrological emulator for global applications – HE v1.0.0. *Geoscientific Model Development*. https://doi.org/10.5194/gmd-11-1077-2018

Liu, Z., & Merwade, V. (2018). Accounting for model structure, parameter and input forcing uncertainty in flood inundation modeling using Bayesian model averaging. *Journal of Hydrology*, *565*, 138–149.

Mak, S., Sung, C.-L., Wang, X., Yeh, S.-T., Chang, Y.-H., Joseph, V. R., et al. (2018). An Efficient Surrogate Model for Emulation and Physics Extraction of Large Eddy Simulations. *Journal of the American Statistical Association*, *113*(524), 1443–1456.

Mason, S. J., & Graham, N. E. (2002). Areas beneath the relative operating characteristics (ROC) and relative operating levels (ROL) curves: Statistical significance and interpretation. *Quarterly Journal of the Royal Meteorological Society*, *128*(584), 2145–2166.

Mayr, E., Hagg, W., Mayer, C., & Braun, L. (2013). Calibrating a spatially distributed

conceptual hydrological model using runoff, annual mass balance and winter mass balance. Journal of Hydrology, 478, 40–49. https://doi.org/10.1016/j.jhydrol.2012

Mckay, M. D., Beckman, R. J., & Conover, W. J. (2000). A Comparison of Three Methods for Selecting Values of Input Variables in the Analysis of Output From a Computer Code. *Technometrics: A Journal of Statistics for the Physical, Chemical, and Engineering Sciences*, *42*(1), 55–61.

McEnery, J., Ingram, J., Duan, Q., Adams, T., & Anderson, L. (2005). NOAA'S ADVANCED HYDROLOGIC PREDICTION SERVICE: Building Pathways for Better Science in Water Forecasting. *Bulletin of the American Meteorological Society*, *86*(3), 375–386.

Mejia, A. I., & Reed, S. M. (2011). Evaluating the effects of parameterized cross section shapes and simplified routing with a coupled distributed hydrologic and hydraulic model. *Journal of Hydrology*, *409*(1), 512–524.

Melsen, L., Teuling, A., Torfs, P., Zappa, M., Mizukami, N., Mendoza, P., Clark, M. P., & Uijlenhoet, R. (2019). Subjective modeling decisions can significantly impact the simulation of flood and drought events. Journal of Hydrology, 568, 1093–1104.

Mendoza, P. A., Clark, M. P., Mizukami, N., Newman, A. J., Barlage, M., Gutmann, E. D., et al. (2015). Effects of Hydrologic Model Choice and Calibration on the Portrayal of Climate Change Impacts. *Journal of Hydrometeorology*, *16*(2), 762–780.

Merz, B., Hall, J., Disse, M., & Schumann, A. (2010). Fluvial flood risk management in a changing world. *Natural Hazards and Earth System Sciences*, *10*(3), 509–527.

Mizukami, N., Rakovec, O., Newman, A. J., Clark, M. P., Wood, A. W., Gupta, H. V., & Kumar, R. (2019). On the choice of calibration metrics for "high-flow" estimation using hydrologic models. *Hydrology and Earth System Sciences*, *23*(6), 2601–2614.

Morzfeld, M., Day, M. S., Grout, R. W., Heng Pau, G. S., Finsterle, S. A., & Bell, J. B. (2018). Iterative Importance Sampling Algorithms for Parameter Estimation. *SIAM Journal of Scientific Computing*, *40*(2), B329–B352.

Murphy, A. H. (1970). THE RANKED PROBABILITY SCORE AND THE PROBABILITY SCORE: A COMPARISON. *Monthly Weather Review*, *98*(12), 917–924.

Murphy, A. H. (1973). A New Vector Partition of the Probability Score. *Journal of Applied Meteorology and Climatology*, *12*(4), 595–600.

Murray, L. M., Lee, A., & Jacob, P. E. (2016). Parallel Resampling in the Particle Filter. *Journal of Computational and Graphical Statistics: A Joint Publication of American Statistical Association, Institute of Mathematical Statistics, Interface Foundation of North America*, *25*(3), 789–805.

Neal, R. M. (2001). Annealed importance sampling. *Statistics and Computing*, *11*(2), 125–139.

Neumann, T., & Ahrendt, K. (2013). Comparing The“ Bathtub Method” With Mike 21 Hd Flow Model For Modelling Storm Surge Inundation. *Ecologic Institute, Berlin, Germany*. Retrieved from https://edoc.sub.uni-hamburg.de/klimawandel/frontdoor/deliver/index/docId/835/file/RADOST_BATHTUB_034.pdf

NWS, 2011: National Weather Service. Hydrology Laboratory-Research Distributed Hydrologic Model (HL-RDHM) user manual, version 3.2.0. NWS Rep., 131 pp.

Oakley, J. E. (2009). Decision-Theoretic Sensitivity Analysis for Complex Computer Models. *Technometrics: A Journal of Statistics for the Physical, Chemical, and Engineering Sciences*, *51*(2), 121–129.

Papaioannou, I., Papadimitriou, C., & Straub, D. (2016). Sequential importance sampling for

structural reliability analysis. *Structural Safety*, *62*, 66–75.

Park, S., Hwang, J. P., Kim, E., & Kang, H.-J. (2009). A New Evolutionary Particle Filter for the Prevention of Sample Impoverishment. *IEEE Transactions on Evolutionary Computation*, *13*(4), 801–809.

Pianosi, F., Beven, K., Freer, J., Hall, J. W., Rougier, J., Stephenson, D. B., & Wagener, T. (2016). Sensitivity analysis of environmental models: A systematic review with practical workflow. *Environmental Modelling & Software*, *79*, 214–232.

Prat, O. P., & Nelson, B. R. (2015). Evaluation of precipitation estimates over CONUS derived from satellite, radar, and rain gauge data sets at daily to annual scales (2002–2012). *Hydrology and Earth System Sciences*. https://doi.org/10.5194/hess-19-2037-2015

Rafieeinasab, A., Norouzi, A., Kim, S., Habibi, H., Nazari, B., Seo, D.-J., et al. (2015). Toward high-resolution flash flood prediction in large urban areas – Analysis of sensitivity to spatiotemporal resolution of rainfall input and hydrologic modeling. *Journal of Hydrology* , *531*, 370–388.

Raje, D., & Krishnan, R. (2012). Bayesian parameter uncertainty modeling in a macroscale hydrologic model and its impact on Indian river basin hydrology under climate change. *Water Resources Research*, *48*(8). https://doi.org/10.1029/2011wr011123

Rajib, A., Liu, Z., Merwade, V., Tavakoly, A. A., & Follum, M. L. (2020). Towards a large-scale locally relevant flood inundation modeling framework using SWAT and LISFLOOD-FP. *Journal of Hydrology*, *581*, 124406.

Razavi, S., & Tolson, B. A. (2013). An efficient framework for hydrologic model calibration on long data periods. *Water Resources Research*, *49*(12), 8418–8431.

Read, L. K., & Vogel, R. M. (2015). Reliability, return periods, and risk under nonstationarity.

Water Resources Research, *51*(8), 6381–6398.

Reed, S., Schaake, J., & Zhang, Z. (2007). A distributed hydrologic model and threshold frequency-based method for flash flood forecasting at ungauged locations. *Journal of Hydrology*, *337*(3), 402–420.

Reed, P. M., Hadjimichael, A., Malek, K., Karimi, T., Vernon, C. R., Srikrishnan, V., et al. (2022). Addressing Uncertainty in MultiSector Dynamics Research. Retrieved from https://uc-ebook.org/

Rojas, M., Quintero, F., & Krajewski, W. F. (2020). Performance of the national water model in Iowa using independent observations. *Journal of the American Water Resources Association*, *56*(4), 568–585.

Ruckert, K. L., Srikrishnan, V., & Keller, K. (2019). Characterizing the deep uncertainties surrounding coastal flood hazard projections: A case study for Norfolk, VA. *Scientific Reports*, *9*(1), 11373.

Sacks, J., Welch, W. J., Mitchell, T. J., & Wynn, H. P. (1989). Design and Analysis of Computer Experiments. *Schweizerische Monatsschrift Fur Zahnheilkunde = Revue Mensuelle Suisse D'odonto-Stomatologie / SSO*, *4*(4), 409–423.

Salas, F. R., Somos-Valenzuela, M. A., Dugger, A., Maidment, D. R., Gochis, D. J., David, C. H., et al. (2018a). Towards real-time continental scale streamflow simulation in continuous and discrete space. *Journal of the American Water Resources Association*, *54*(1), 7–27.

Salas, J. D., Obeysekera, J., & Vogel, R. M. (2018b). Techniques for assessing water infrastructure for nonstationary extreme events: a review. *Hydrological Sciences Journal*, *63*(3), 325–352.

Sanders, B. F., Schubert, J. E., Goodrich, K. A., Houston, D., Feldman, D. L., Basolo, V., et al.

(2020). Collaborative Modeling With Fine-Resolution Data Enhances Flood Awareness, Minimizes Differences in Flood Perception, and Produces Actionable Flood Maps. *Earth's Future*. https://doi.org/10.1029/2019ef001391

Scawthorn, C., Blais, N., Seligson, H., Tate, E., Mifflin, E., Thomas, W., et al. (2006). HAZUS-MH flood loss estimation methodology. I: Overview and flood hazard characterization. *Natural Hazards Review*, *7*(2), 60–71.

Shafii, M., Tolson, B., & Shawn Matott, L. (2015). Addressing subjective decision-making inherent in GLUE-based multi-criteria rainfall–runoff model calibration. *Journal of Hydrology*, *523*, 693–705.

Sharma, S., Siddique, R., Reed, S., Ahnert, P., & Mejia, A. (2019). Hydrological model diversity enhances streamflow forecast skill at short- to medium-range timescales. *Water Resources Research*, *55*(2), 1510–1530.

Sharma, S., Gomez, M., Keller, K., Nicholas, R., & Mejia, A. (2021). Regional Flood Risk Projections under Climate Change. *Journal of Hydrometeorology*, *-1*(aop). https://doi.org/10.1175/JHM-D-20-0238.1

Siddique, R., & Mejia, A. (2017). Ensemble Streamflow Forecasting across the U.S. Mid-Atlantic Region with a Distributed Hydrological Model Forced by GEFS Reforecasts. *Journal of Hydrometeorology*, *18*(7), 1905–1928.

Smith, T., Marshall, L., & Sharma, A. (2015). Modeling residual hydrologic errors with Bayesian inference. Journal of Hydrology, 528, 29-37.

Sorooshian, S., Q. Y. Duan, and V. K. Gupta (1993), Calibration of rainfall-runoff models—Application of global optimization to the Sacramento soil-moisture accounting model, Water Resour. Res., 29(4), 1185–1194, doi:10.1029/92WR02617.

Stein, M. (1987). Large Sample Properties of Simulations Using Latin Hypercube Sampling. *Technometrics: A Journal of Statistics for the Physical, Chemical, and Engineering Sciences*, *29*(2), 143–151.

Steinberg, D. M., & Lin, D. K. J. (2006). A construction method for orthogonal Latin hypercube designs. *Biometrika*. https://doi.org/10.1093/biomet/93.2.279

Stedinger, J. R., R. M. Vogel, S. U. Lee, and R. Batchelder (2008), Appraisal of the generalized likelihood uncertainty estimation (GLUE) method, Water Resour. Res., 44, W00B06, doi:10.1029/2008WR006822.

Storn, R., & Price, K. (1997). *Journal of Global Optimization*, *11*(4), 341–359.

Su, Y., Feng, Q., Zhu, G., Gu, C., Wang, Y., Shang, S., et al. (2018). A hierarchical Bayesian approach for multi-site optimization of a satellite-based evapotranspiration model. *Hydrological Processes*, *32*(26), 3907–3923.

Tang, Y., Marshall, L., Sharma, A., & Smith, T. (2016). Tools for investigating the prior distribution in Bayesian hydrology. Journal of Hydrology, 538, 551-562.

Tarawneh, E., Bridge, J., & Macdonald, N. (2016). A pre-calibration approach to select optimum inputs for hydrological models in data-scarce regions. *Hydrology and Earth System Sciences*. https://doi.org/10.5194/hess-20-4391-2016

Tellman, B., Sullivan, J. A., Kuhn, C., Kettner, A. J., Doyle, C. S., Brakenridge, G. R., et al. (2021). Satellite imaging reveals increased proportion of population exposed to floods. *Nature*, *596*(7870), 80–86.

Vrugt, J. A., H. V. Gupta, W. Bouten, and S. Sorooshian (2003), A Shuffled Complex Evolution Metropolis algorithm for optimization and uncertainty assessment of hydrologic model parameters, Water Resour. Res., 39(8), 1201, doi:10.1029/2002WR001642.

Vrugt, J. A., C. J. F.ter Braak, C. G. H.Diks, B. A.Robinson, J. M.Hyman, and D.Higdon (2009), Accelerating Markov Chain Monte Carlo simulation by differential evolution with self-adaptive randomized subspace sampling, Int. J. Nonlinear Sci. Numer. Simul., 10(3), 273–290.

Vrugt, J. A., C. J. F. ter Braak, M. P. Clark, J. M. Hyman, and B. A. Robinson (2008), Treatment of input uncertainty in hydrologic modeling: Doing hydrology backward with Markov chain Monte Carlo simulation, Water Resour. Res., 44, W00B09, doi:10.1029/2007WR006720.

Wasko, C., Westra, S., Nathan, R., Orr, H. G., Villarini, G., Villalobos Herrera, R., & Fowler, H. J. (2021). Incorporating climate change in flood estimation guidance. *Philosophical Transactions. Series A, Mathematical, Physical, and Engineering Sciences*, *379*(2195), 20190548.

Williamson, D. B., Blaker, A. T., & Sinha, B. (2017). Tuning without over-tuning: parametric uncertainty quantification for the NEMO ocean model, Geosci. Model Dev., 10, 1789–1816, https://doi.org/10.5194/gmd-10-1789-2017, 2017.

Wing, O. E. J., Bates, P. D., Smith, A. M., Sampson, C. C., Johnson, K. A., Fargione, J., & Morefield, P. (2018). Estimates of present and future flood risk in the conterminous United States. *Environmental Research Letters: ERL [Web Site]*, *13*(3), 034023.

Wing, O. E. J., Pinter, N., Bates, P. D., & Kousky, C. (2020). New insights into US flood vulnerability revealed from flood insurance big data. *Nature Communications*, *11*(1), 1444.

Winsemius, H. C., Jeroen C J, van Beek, L. P. H., Bierkens, M. F. P., Bouwman, A., Jongman, B., et al. (2015). Global drivers of future river flood risk. *Nature Climate Change*, *6*(4), 381–385.

Wong, T. E., & Keller, K. (2017). Deep Uncertainty Surrounding Coastal Flood Risk

Projections: A Case Study for New Orleans. *Earth's Future*. https://doi.org/10.1002/2017ef000607

Yunus, A. P., Avtar, R., Kraines, S., Yamamuro, M., Lindberg, F., & Grimmond, C. S. B. (2016). Uncertainties in Tidally Adjusted Estimates of Sea Level Rise Flooding (Bathtub Model) for the Greater London. *Remote Sensing*, *8*(5), 366.

Zarekarizi, M., Srikrishnan, V., & Keller, K. (2020). Neglecting uncertainties biases house-elevation decisions to manage riverine flood risks. *Nature Communications*, *11*(1), 5361.

Zarzar, C. M., Hosseiny, H., Siddique, R., Gomez, M., Smith, V., Mejia, A., & Dyer, J. (2018). A hydraulic MultiModel ensemble framework for visualizing flood inundation uncertainty. *Journal of the American Water Resources Association*, *54*(4), 807–819.

Zhu, G., Li, X., Ma, J., Wang, Y., Liu, S., Huang, C., et al. (2018). A new moving strategy for the sequential Monte Carlo approach in optimizing the hydrological model parameters. *Advances in Water Resources*, *114*, 164–179.